

Activation of histamine type 2 receptors enhances intrinsic excitability of medium spiny neurons in the nucleus accumbens

Giuseppe Aceto^{1,2} , Luca Nardella², Simona Nanni^{1,3}, Valeria Pecci³, Alessia Bertozzi⁴, Claudia Colussi^{1,4}, Marcello D'Ascenzo^{1,2}  and Claudio Grassi^{1,2}

¹Fondazione Policlinico Universitario Agostino Gemelli, IRCCS, Rome, Italy

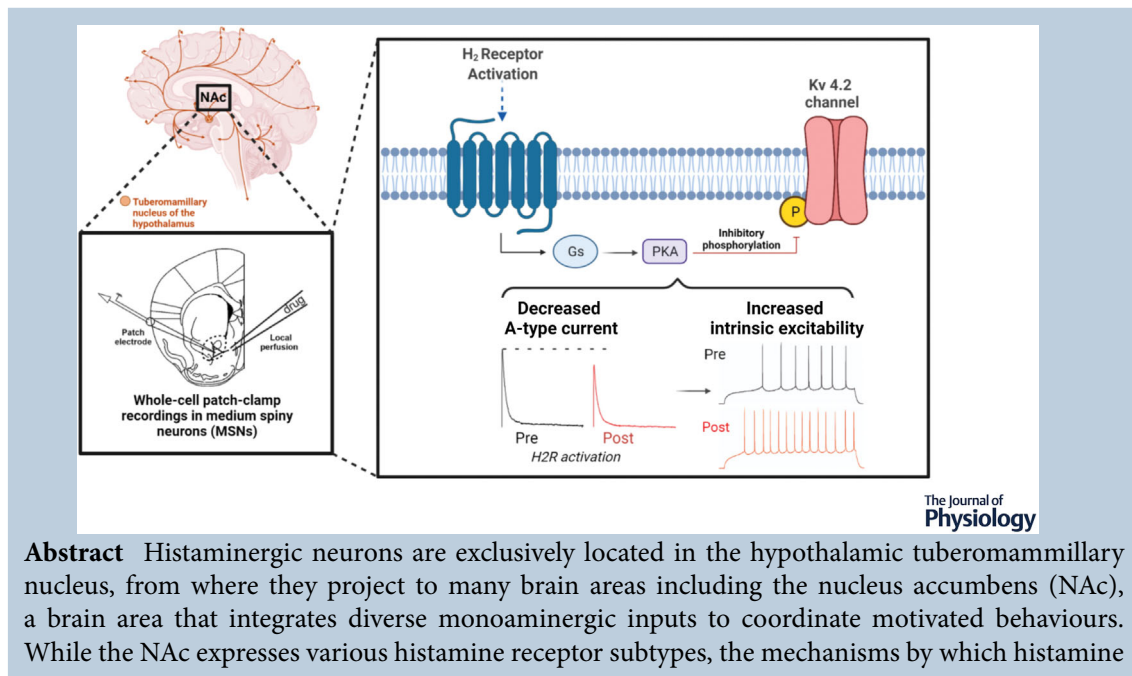
²Department of Neuroscience, Università Cattolica del Sacro Cuore, Rome, Italy

³Department of Translational Medicine and Surgery, Università Cattolica del Sacro Cuore, Rome, Italy

⁴Istituto di Analisi dei Sistemi ed Informatica "Antonio Ruberti" National Research Council, Rome, Italy

Edited by: David Wyllie & Tommas Ellender

The peer review history is available in the Supporting Information section of this article (<https://doi.org/10.1113/JP282962#support-information-section>).



Abstract Histaminergic neurons are exclusively located in the hypothalamic tuberomammillary nucleus, from where they project to many brain areas including the nucleus accumbens (NAc), a brain area that integrates diverse monoaminergic inputs to coordinate motivated behaviours. While the NAc expresses various histamine receptor subtypes, the mechanisms by which histamine

Giuseppe Aceto, PhD, is a Research Fellow working at the laboratory of Prof. Claudio Grassi, at the Fondazione Policlinico Universitario A. Gemelli IRCCS in Rome. By performing electrophysiological and behavioural experiments, he recently identified a GSK3-mediated mechanism underlying vulnerability to depression relying on altered synaptic plasticity in the nucleus accumbens of mice. He is currently investigating the mechanisms by which chronic stress alters histaminergic transmission in mice. **Luca Nardella** is a PhD student in Neuroscience under the supervision of Prof. Marcello D'Ascenzo at Università Cattolica del Sacro Cuore in Rome. His research interest concerns regulatory mechanisms by which chronic stress alters histaminergic transmission in mice.



G. Aceto and L. Nardella contributed equally to this work.

M. D'Ascenzo and C. Grassi shared senior authorship.

modulates NAc activity are still poorly understood. Using whole-cell patch-clamp recordings, we found that pharmacological activation of histamine 2 (H2) receptors elevates the excitability of NAc medium spiny neurons (MSNs), while activation of H1 receptors failed to significantly affect MSN excitability. The evoked firing of MSNs increased after seconds of local H2 agonist administration and remained elevated for minutes. H2 receptor (H2R) activation accelerated sub-threshold depolarization in response to current injection, reduced the latency to fire, diminished action potential afterhyperpolarization and increased the action potential half-width. The increased excitability was protein kinase A-dependent and associated with decreased A-type K⁺ currents. In addition, selective pharmacological inhibition of the Kv4.2 channel, the main molecular determinant of A-type K⁺ currents in MSNs, mimicked and occluded the increased excitability induced by H2R activation. Our results indicate that histaminergic transmission in the NAc increases MSN intrinsic excitability through H2R-dependent modulation of Kv4.2 channels. Activation of H2R will significantly alter spike firing in MSNs *in vivo*, and this effect could be an important mechanism by which these receptors mediate certain aspects of goal-induced behaviours.

(Received 14 February 2022; accepted after revision 21 March 2022; first published online 28 March 2022)

Corresponding author Marcello D'Ascenzo: Department of Neuroscience, Università Cattolica del Sacro Cuore, Largo Francesco Vito 1, 00168 Rome, Italy. Email: marcello.dascenzo@unicatt.it

Abstract figure legend Pharmacological activation of histamine receptor type 2 (H2R) elevates the frequency of evoked firing in medium spiny neurons (MSNs) of the nucleus accumbens (NAc). The mechanism underlying this effect requires protein kinase A-dependent phosphorylation and downregulation of Kv4.2 channels, the molecular determinant of A-type K⁺ currents.

Key points

- Histamine is synthesized and released by hypothalamic neurons of the tuberomammillary nucleus and serves as a general modulator for whole-brain activity including the nucleus accumbens.
- Histamine receptors type 2 (HR2), which are expressed in the nucleus accumbens, couple to G α s/off proteins which elevate cyclic adenosine monophosphate levels and activate protein kinase A.
- Whole-cell patch-clamp recordings revealed that H2R activation increased the evoked firing in medium spiny neurons of the nucleus accumbens via protein kinase A-dependent mechanisms.
- HR2 activation accelerated subthreshold depolarization in response to current injection, reduced the latency to fire, diminished action potential medium after-hyperpolarization and increased the action potential half-width. HR2 activation also reduced A-type potassium current.
- Selective pharmacological inhibition of the Kv4.2 channel mimicked and occluded the increased excitability induced by H2R activation.

Introduction

The nucleus accumbens (NAc) is the main component of the ventral striatum and a major input structure of the basal ganglia integrating information from the cortical, allocortical, thalamic, midbrain and brain-stem structures to mediate goal-directed behaviours (Groenewegen et al., 1999; Scofield et al., 2016). The majority of NAc inputs arise from glutamatergic afferents including the prefrontal cortex (PFC), the basolateral amygdala (BLA) and the ventral hippocampus (vHipp), whereas the ventral tegmental area (VTA) and the ventral pallidum (VP) provide GABAergic inputs. The NAc is

also heavily innervated by dopaminergic neurons of the VTA that mediates the association of motor actions with action outcomes, as necessary for individuals to repeat behaviours that lead to good outcomes (Bromberg-Martin et al., 2010; Steinberg et al., 2014). In addition, the NAc is regulated by various neuromodulators such as serotonin, orexin and histamine (HA) (Dolen et al., 2013; Ellenbroek & Ghiabi, 2014; Nevarez & de Lecea, 2018). While the monoaminergic influence on the mesocorticolimbic system is well characterized, less is known about how HA, a non-canonical monoamine, contributes to NAc functions. HA is synthesized and released by L-histidine decarboxylase-expressing hypothalamic neurons of the

tuberomammillary nucleus (TMN) and serves as a general modulator for whole-brain activity through HA1–4 receptors (Panula & Nuutinen, 2013). The action of HA in the brain mediates sleep–wake transition, attention, wakefulness, appetite and motivational behaviours. Accordingly, dysregulation in HA signalling is associated with sleep, cognitive, motor and psychiatric disorders (Panula & Nuutinen, 2013). Multiple HA receptors are expressed in medium spiny neurons (MSNs) of the NAc including the postsynaptically expressed HA receptor type 1 (H1R) and H2R (Shoblock & O'Donnell, 2000). H2Rs, which are highly expressed in the NAc, couple to $G\alpha_{s/off}$ protein, which, through their stimulation of adenylyl cyclase, elevate cyclic adenosine monophosphate (cAMP) levels and activate protein kinase A (PKA). H1Rs, instead, couple to $G\alpha_q/11$ proteins, which stimulate phospholipase C and promote: (1) inositol trisphosphate (IP3)-dependent release of Ca^{2+} from intracellular stores and (2) diacylglycerol (DAG)-sensitive activation of protein kinase C (PKC). Both H1R and H2R pathways have the potential to modulate a variety of intracellular targets, including ion channels that regulate neuronal excitability. However, very little is known about the effects of H1R and H2R signalling on MSN function. Here we sought to fill this gap by asking whether, and through which mechanism, HRs affect NAc MSN intrinsic excitability. We found that only H2R activation powerfully enhances MSN firing through PKA-dependent modulation of A-type potassium currents carried by Kv4.2 channels.

Materials and methods

Animal and ethical approval

Male C57BL/6J mice, bred in house, were maintained on a 12-h light/dark cycle, in a temperature- and humidity-controlled room with *ad libitum* access to mouse chow and water. Four- to 5-week-old mice were used. All animal procedures were approved by the Ethics Committee of the Catholic University and complied with Italian Ministry of Health guidelines, national laws (Legislative Decree 116/1992; Ethics approval number: 766/2021-PR) and European Union guidelines on animal research (No. 86/609/EEC).

Slice preparation and electrophysiology

Coronal slices (300 μm) containing the NAc were prepared as previously described (Mainardi et al., 2017; Scala et al., 2015). C57/BL/6J mice -postnatal days (P)21–60] were anaesthetized with isoflurane, killed by cervical dislocation and decapitated. The brains were rapidly removed and placed in ice-cold, sucrose-based cutting

solution containing the following (in mM): Tris-HCl 72, TRIZMA base 18, NaH_2PO_4 1.2, NaHCO_3 30, KCl 2.5, glucose 25, Hepes 20, MgSO_4 10, sodium pyruvate 3, ascorbic acid 5, CaCl_2 0.5, sucrose 20. NAc slices (300 μm thick) were cut on a vibratome (VT1200S; Leica Microsystems, Wetzlar, Germany) and immediately transferred to an incubation chamber held at 32°C and filled with a recovery solution containing (in mM): Tris-HCl 72, TRIZMA base 18, NaH_2PO_4 1.2, NaHCO_3 25, KCl 2.5, glucose 25, Hepes 20, MgSO_4 10, sodium pyruvate 3, ascorbic acid 5, CaCl_2 0.5, sucrose 20. After 30 min, slices were transferred to a second incubation chamber held at 32°C and filled with artificial cerebrospinal fluid (aCSF) containing the following (in mM): NaCl 124, KCl 3.2, NaH_2PO_4 1.2, MgCl_2 1, CaCl_2 2, NaHCO_3 26 and glucose 10, pH 7.4. During incubations, the chambers were continuously bubbled with 95% O_2 /5% CO_2 . Finally, slices were equilibrated at room temperature for at least 45 min. For electrophysiological recordings, slices were transferred to a submerged recording chamber constantly perfused with heated aCSF (32°C) and bubbled with 95% O_2 /5% CO_2 . MSNs of the NAc were visualized under differential interference contrast (DIC) infrared illumination. Patch pipettes had a resistance of 4–6 M Ω when filled with an internal solution containing (in mM): potassium gluconate 145, MgCl_2 2, Hepes 10, EGTA 0.1, Na-ATP 2.5, Na-GTP 0.25, phosphocreatine 5, pH adjusted to 7.2 with KOH.

Recordings were performed using a Multiclamp 700B/Digidata 1550A system (Molecular Devices, Sunnyvale, CA, USA) and digitized at a sampling frequency of 10 000 Hz. All the electrophysiological recordings were analysed using the Clampfit 10.9 software (Molecular Devices). Evoked firings were recorded in whole-cell, current-clamp mode. Only cells with a stable resting membrane potential negative to -80 mV, overshooting action potentials (exceeding 75–80 mV threshold-to-peak) and an input resistance >100 M Ω were included. Furthermore, cells were rejected if resting membrane potential and input resistance changed by more than 20%. The membrane input resistance was measured by a series of 600 ms hyperpolarizing current steps from -50 to 0 pA, 10 pA steps with 1 s interval.

To test the firing properties of MSNs during continuous depolarization, we exposed these cells to a series of 1 s somatic current pulses (every 5 s). Current levels were chosen based on minimum amplitudes required to elicit a stable firing of 4–8 action potentials. Beginning at 80 pA, the injected current was gradually increased in 10–50 pA increments until these criteria were satisfied. Of note, during interpulse intervals, membrane potentials were kept at the resting value (~ 80 mV) by injecting hyperpolarizing/depolarizing currents to counteract possible H2R-dependent depolarization (Zhuang et al., 2018). Local exposure of the recorded MSN to 10 μM dimaprit

(for 1 min) was achieved by pacing a glass pipette ($\sim 5 \mu\text{m}$ tip diameter) 40–100 μm away from the cell body with continuous pressure of ~ 0.5 –1 psi. All the electrophysiological parameters were analysed 10–30 s (pre) and 1–2 min (post) application of drugs.

Action potential threshold values were calculated from waveform averages by determining the first point of sustained positive acceleration (second derivative) of voltage that exceeded 2 SDs of the acceleration 'noise' 5–10 ms prior to threshold. Measurements of action potential half-width and all action potential properties were taken from waveform averages representing 1 s per condition. Afterhyperpolarization voltages were measured individually from raw traces prior to averaging.

The transient A-type K^+ current in voltage-clamp mode was recorded applying 400 ms voltage steps from -110 to $+40$ mV. A prepulse of hyperpolarization at -110 mV for 100 ms removed A-type K^+ channel inactivation and enabled subsequent maximum activation. The transient channel was inactivated by the same voltage steps that preceded a depolarizing prepulse of -10 mV for 100 ms, leaving the sustained current of the total outward current. The transient current was then isolated by a digital subtraction of the sustained current from the total outward current. To record A-type K^+ current, the following reagents were added to the external solution: 1 μM TTX, 300 μM Cd^{2+} and 20 mM of tetraethylammonium (TEA). Excitatory and inhibitory synaptic transmission were also blocked using NBQX (10 μM) and picrotoxin (50 μM). Membrane capacitances and series resistances (R_s) were compensated electronically. R_s before compensation were in the range 5–20 $\text{M}\Omega$ and were routinely corrected by 75–85%. Data obtained from a given cell were rejected if R_s were larger than $>20 \text{M}\Omega$ or changed by $>20\%$ during the course of the experiment.

Analysis and curve fitting were conducted in Clampfit 10.9 (Molecular Devices) and SigmaPlot 14.0 (Systat Software Inc., San Jose, CA, USA). The peak conductance (G_p) was calculated as $G_p = I_p / (V_c - V_{\text{rev}})$, where I_p is the peak outward current, V_c is the command voltage and V_{rev} is the estimated reversal potential for K^+ (-95 mV). The G_p – V relationships were described assuming a first-order Boltzmann function: $G_p(V) = G_{\text{pmax1}} / (1 + \exp((V_c - V_{1/2a})/ka))$, where G_{pmax1} is the maximal peak conductance, ka is the slope factor and $V_{1/2a}$ is the activation midpoint voltage. Steady-state inactivation curves, obtained based on recordings performed using the protocol shown in Fig. 6E, were described assuming a first-order Boltzmann function plus a constant.

Western-blot assay

Tissues were lysed in ice-cold lysis buffer (NaCl 150 mM, Tris-HCl 50 mM pH 7.4, EDTA 2 mM) containing 1%

Triton X-100, 0.1% SDS, 1 \times protease inhibitor cocktail (Sigma-Aldrich, St Louis, MO, USA), 1 mM sodium orthovanadate (Sigma-Aldrich) and 1 mM sodium fluoride (Sigma-Aldrich). Lysates were incubated for 10 min on ice with occasional vortexing and spun down at 22 000 g and 4°C. The supernatant was quantified for protein content (DC Protein Assay; Bio-Rad, Hercules, CA, USA). Equal amounts of protein were diluted in Laemmli buffer, boiled and resolved by SDS-PAGE. Primary antibodies for anti-Kv4.2 (WB 1:1000, monoclonal, Origene 75-016), anti-H1R (WB 1:1000, monoclonal, Santa Cruz, sc-374621; Santa Cruz, CA, USA), anti-H2R (WB 1:1000, goat, Everest Biotech, EB06905; Bicester, UK), anti-beta-actin (WB 1:2000, polyclonal, Abcam ab8227; Cambridge, MA, USA) and anti-PSD95 (WB 1:1000, polyclonal, Cell Signaling 3550; Danvers, MA, USA) were incubated overnight and revealed with HRP-conjugated secondary antibodies (Cell Signaling Technology). Expression was evaluated and documented by using UVitec Cambridge Alliance. Images shown were cropped for presentation with no manipulations. For the western blot experiment reported in Fig. 1C and D, statistical comparison was not performed due to different affinity and specificity of H1R and H2R antibodies for their relative targets.

Cellular fractioning

Brain slices were suspended in Syn-PER reagent (Thermo Fisher, Waltham, MA, USA) containing protease and phosphatase inhibitors (Sigma-Aldrich) to specifically separate intact membranes from cytosol. Tissues were gently homogenized in a pre-chilled Dounce tissue grinder with 10 slow strokes and the lysate was centrifuged at 1200 g for 10 min at 4°C. The pellet was discarded and the supernatant centrifuged at 15 000 g for 20 min at 4°C. The supernatant, containing the cytosolic fraction, was saved for western blotting analysis and the pellet, containing the membrane fractions, was resuspended in RIPA buffer plus 0.1% SDS and vortexed for 15 s every 10 min for a total of 40 min to dissolve the proteins. Extracts were quantified (Bio-Rad) and analysed by western blotting.

RNA extraction and RT-PCR

RNA was extracted from mouse NAc and cortex (Ctx) tissues using Trizol after tissue homogenization (homogenizer VDI12, VWR). RNA extraction, cDNA preparation and real-time PCR with Syber Green on QuantStudio 5 System (Applied Biosystems, Foster City, CA, USA) was performed as in Possieri et al. (2021). Primers are as follows: HRH1 F 5'-CATCACTCCCTAGGACAGCC-3', R 5'-GTCCTGTTCCCCTCACACAT-3'; HRH2 F 5'-AGCTCCTATGACC

CCAGAAAGAGT-3', R 5'-TGGTGCCTGTTTCCATCG A-3'; KCND2 F 5'-GGCAGCCTTCTGGTACACCAT-3'; R 5'-GCACGGGTAGCGCAATG-3'; GAPDH F 5'-TGC ACCACCACCTGCTTAGC-3', R 5'-GTCTTCTGGGTG GCAGTGATG-3'.

Droplet digital PCR analysis (ddPCR)

Serial cDNA dilution for NAc tissues (from 1:5 to 1:400) was used to set up ddPCR assays performed as previously described (Possieri et al., 2021). The intracellular contents (~4–5 μ l) were drawn into the tip of the patch pipette by applying negative pressure and were then transferred to RNase/DNase-free tubes (Cadwell et al., 2017) and processed as in Possieri et al. (2021) with some modifications. Briefly, cells were lysed in 5 μ l of lysis buffer according to the manufacturer's instructions (Single Shot Cell Lysis Kit, Bio-Rad) and subjected to reverse transcription using a High Capacity Kit (Applied Biosystems). The preamplification step was performed using 4 μ l of cDNA with Eva green 2 \times reaction and primer mix at 50 nM final concentration (PCR: 14 cycles at 95°C for 15 s and at 58°C for 4 min). Eight microlitres preAmp (1:10 dilution) were used to perform ddPCR in duplicate with EVA green, giving a total droplet number >14 000. Data are quantified as copy number μ l. mRNA levels were normalized to housekeeping genes GAPDH and/or β Actin. The data in Fig. 1A and Fig. 9G are represented as box plots showing median, upper and lower quartiles of the data and minimum and maximum values as whiskers.

Statistical analysis

Throughout this study, data are shown as means \pm SD and the number of cells (n) and mice (N) are indicated. Data were averaged for each mouse used, unless otherwise indicated. Data in the figures are plotted showing both single cells and averaged data for each studied mouse. Statistical significance was assessed with either Student's t test or one-factor ANOVA for multiple-group comparisons (with the Bonferroni *post hoc* test). Statistical analysis was performed with the SYSTAT 10.2 software (Systat Software, Chicago, IL, USA). Two-tailed, non-parametric statistical comparisons were performed using the Wilcoxon signed-rank (WSR) test for paired data or the Mann–Whitney U (MWU) test for unpaired data. The level of significance was set at 0.05.

Results

Pharmacological activation of HR2 enhances evoked firing of MSNs through a PKA-dependent mechanism

We first sought to profile the expression of H1R and H2R in MSNs of the NAc by using a single cell approach. For

this, we assessed H2R and H1R mRNA levels in MSNs using a protocol that combines whole-cell patch-clamp recordings with high-quality single cell RNA analysis by ddPCR (single-cell qRT-ddPCR) (Cadwell et al., 2016; Possieri et al., 2021). As shown in Fig. 1A, the vast majority of screened MSNs expressed both H2R and H1R subtypes (H2R: 18/20; H1R: 15/20). However, the levels of mRNA for H2R were significantly higher compared to those attributable to H1R, a finding that was also confirmed in NAc tissues (Fig. 1B). Accordingly, a similar picture in H2R vs. H1R protein levels was found in NAc tissues by semi-quantitative western blot analysis (Fig. 1C and D). These results suggest that H2R is the prevailing post-synaptic histamine receptor in NAc MSNs.

To determine the effects of H2R activation on MSN excitability, we performed whole-cell patch-clamp recordings of identified NAc MSNs in *ex vivo* brain slices during local perfusion of dimaprit (10 μ M), a selective agonist of H2R (Fig. 2A and B). In addition to morphological criteria (e.g. somatic diameter of 10–15 μ m), MSNs, which represent >95% of the

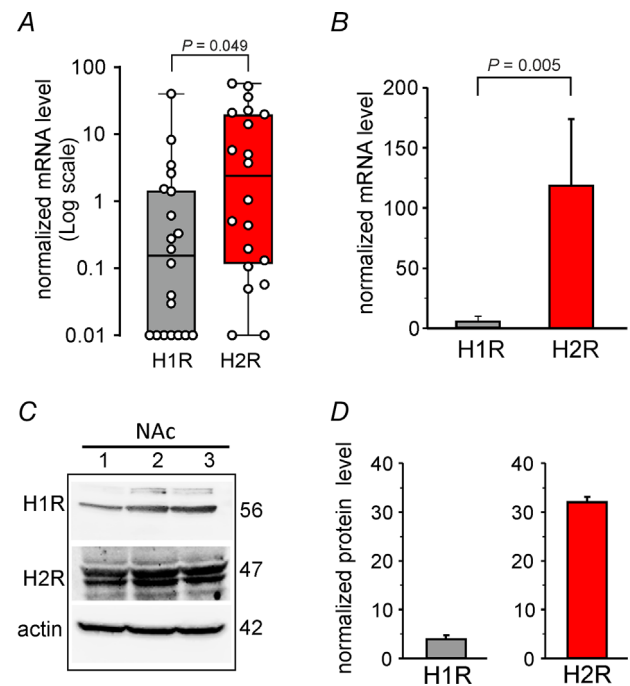


Figure 1. Expression of histamine H1R and H2R receptors in single MSNs and NAc tissues

A and B, quantification of H1R and H2R mRNA levels by droplets digital PCR (ddPCR) in single neurons (A) and NAc tissues (B). Data from single neurons (MSNs; $n = 20$ from nine mice) isolated from NAc are represented as a box plot (see Material and Methods). Data from NAc tissues are expressed as mean \pm standard deviation (SD) of three independent experiments each performed in duplicate. C, representative western blots of NAc tissues showing H1R and H2R protein levels. D, densitometric analysis for the blots probed with anti-H1R and anti-H2R and normalized to total actin ($N = 3$ mice). [Colour figure can be viewed at wileyonlinelibrary.com]

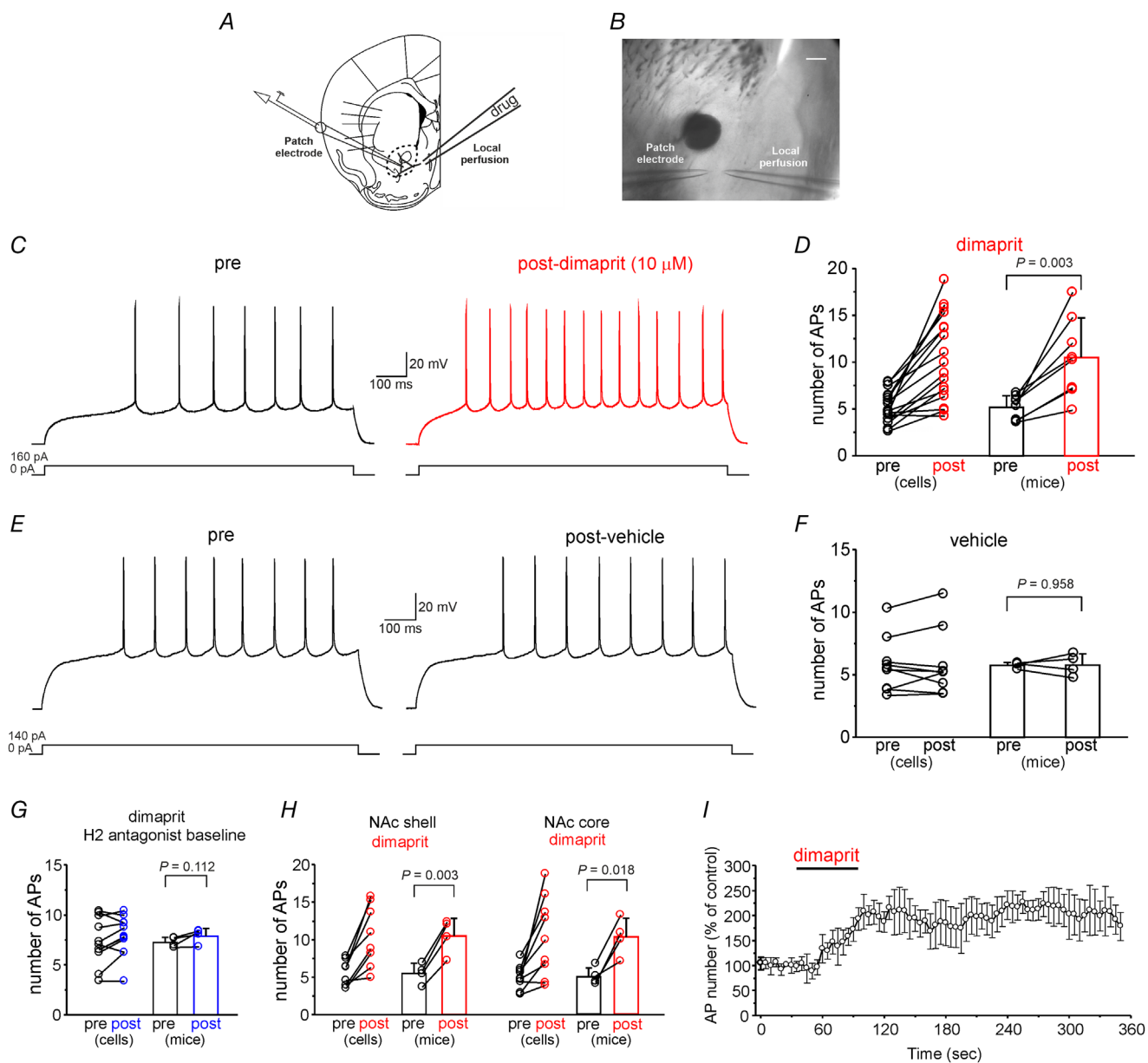


Figure 2. Pharmacological activation of H2R elevates the frequency of evoked firing in MSNs

A, schematic diagram of a brain section at the NAc level with the patch pipette located in the MSN soma and the local perfusion system located 40–100 μm away from the recording electrode. *B*, micrograph indicating the position of the patch recording pipette and the perfusion pipette. Scale bar: 200 μm . *C*, representative traces showing current-evoked firing of an MSN before (black) and after 1 min (red) local perfusion of H2R agonist (dimaprit; 10 μM). The current-evoked firing protocol is depicted at the bottom. *D*, bar graph depicting quantification of evoked firing in the experimental conditions shown in *C*. The bar histograms on the right summarize data collected in each mouse, where each point represents the mean of the subset of data points for the corresponding mouse. Data of each recording are shown on the left. Bars represent normalized mean \pm SD ($N = 8$ mice; $P = 0.0031$; paired Student's t test; $n = 17$ cells). *E* and *F*, representative traces (*E*) and summary plot (*F*) illustrating that vehicle application did not affect evoked firing ($N = 4$ mice; $P = 0.958$; paired Student's t test; $n = 9$ cells), shown as in *B*. *G*, bar graph showing that evoked firing was not affected by dimaprit in slices pre-incubated (5–20 min) with the H2R antagonist ranitidine ($N = 4$ mice; $P = 0.112$; $n = 11$ cells). *H*, bar graph depicting quantification of dimaprit-induced increase of evoked firing in MSNs of the NAc shell and core. *I*, normalized changes in the number of APs before and after 1 min of cell exposure to dimaprit ($N = 4$ mice; $n = 9$ cells). [Colour figure can be viewed at wileyonlinelibrary.com]

neurons in the NAc, were identified by the following electrophysiological features: (1) hyperpolarized resting membrane potential; (2) ramp depolarization at sub-threshold levels; and (3) regular action potential (AP) firing when stimulated with over-threshold voltages. A few cells (~2%) exhibited higher discharge rates than those of most cells and large fast afterhyperpolarizations – features that are typical of fast-spiking GABAergic interneurons (Plenz & Kitai, 1998). They were excluded from further investigation.

To test the firing properties of MSNs during long-lasting depolarization, we applied 1 s somatic current pulses every 5 s. Currents levels were chosen based on minimum amplitudes required to elicit a stable firing of 4–8 APs. Dimaprit was locally applied for 1 min through a pipette (~5 μm tip diameter) placed in the vicinity (40–100 μm) of the MSN being recorded (Fig. 2A and B). Under these experimental conditions, dimaprit robustly increased the evoked firing in NAc MSNs (number of APs: pre = 5.15 ± 1.27 ; post = 10.50 ± 4.18 ; $N = 8$ mice; $P = 0.003$; paired Student's t test; $n = 17$ cells; Fig. 2C and B), an effect that was absent when aCSF (vehicle) was applied (number of APs: pre = 5.76 ± 0.22 ; post = 5.78 ± 0.88 ; $N = 4$ mice; $P = 0.958$; paired Student's t test; $n = 9$ cells; Fig. 2E and F). Prior application of the H2 antagonist ranitidine (100 μM) blocked the action of dimaprit (Fig. 2G; number of APs: pre = 7.26 ± 0.51 ; post = 7.89 ± 0.75 ; $N = 4$ mice; $P = 0.112$; paired Student's t test; $n = 11$ cells), confirming that the dimaprit-induced increase in evoked firing occurred through H2R activation. Of note, dimaprit's effect on evoked firing was independent of MSN localization in NAc core and shell (Fig. 2H; NAc shell; number of APs: pre = 5.49 ± 1.35 ; post = 10.49 ± 2.34 ; $N = 4$ mice; $P = 0.003$; paired Student's t test; $n = 8$ cells; NAc core; number of APs: pre = 5.05 ± 1.19 ; post = 10.27 ± 2.54 ; $N = 4$ mice; $P = 0.018$; paired Student's t test; $n = 9$ cells).

The enhancement of spike-firing developed quite rapidly and peaked at ~60 s of dimaprit application

(Fig. 2I). MSN excitability was persistently elevated for at least 4–5 min following dimaprit application, a feature that may indicate the involvement of PKA-mediated protein phosphorylation (Gervasi et al., 2007; Ma et al., 2018). To test this hypothesis, we bath applied a cell-permeable peptide inhibitor of PKA, PKI 14-22 amide, myristoylated (PKI 1 μM), for at least 10 min prior to dimaprit application. In the presence of PKI, H2R activation failed to significantly affect MSN firing rates (Fig. 3; number of APs: pre = 5.92 ± 1.65 ; post = 6.20 ± 1.70 ; $N = 5$ mice; $P = 0.072$; paired Student's t test; $n = 12$ cells).

H2R activation has been shown to cause inward currents (Zhuang et al., 2018) and membrane depolarization (Ellender et al., 2011) in striatal MSNs. We therefore tested whether these effects could also be observed in NAc MSNs. In voltage-clamp recordings performed at a holding potential of -80 mV, slice superfusion with dimaprit elicited slow, tonic, inward currents (-61.60 ± 23.85 pA; $N = 5$ mice; Fig. 4A and B; $n = 10$ cells). Moreover, in current-clamp recordings, slice perfusion with dimaprit caused mild depolarization of MSNs (from -80.88 ± 0.83 to -75.72 ± 1.57 mV, $N = 4$ mice; $P = 0.005$; $n = 8$ cells). Notably, this H2R-mediated effect on the resting conductances was not related to the increased evoked firing we observed because the membrane potential was kept, during interpulse intervals, at the resting value (~ -80 mV) by injecting hyperpolarizing currents.

We next examined the effects of H1R activation on MSN-evoked firing. As shown in Fig. 5A and B, local application of H1R agonist 2PyEA (100 μM) did not significantly affect firing properties (number of APs: pre = 8.09 ± 1.63 ; post = 9.03 ± 2.25 ; $N = 5$ mice; $P = 0.056$; paired Student's t test; $n = 13$ cells). Finally, we hypothesized that pharmacological blockade of H2R would counteract the histamine-induced increase in evoked firing. In accordance with our hypothesis, evoked firing was significantly increased by histamine

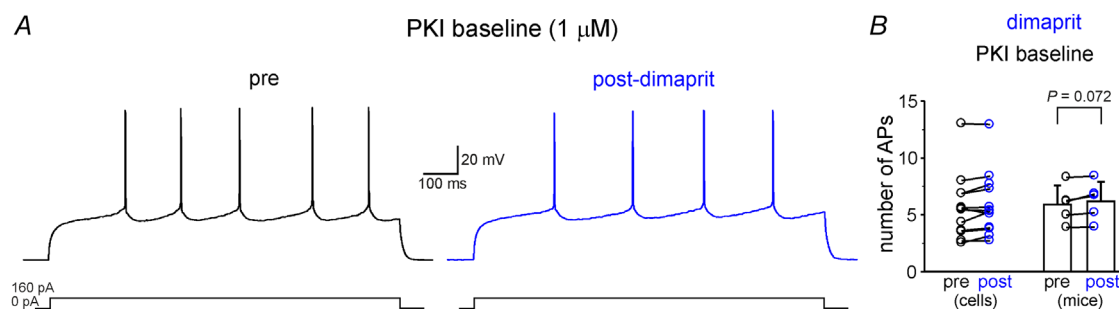


Figure 3. H2R-dependent modulation of evoked firing requires PKA signalling

A, representative traces showing that H2R-dependent modulation of evoked firing was not observed when slices were pre-incubated (5–20 min) with the PKA inhibitors PKI-14-22 amide, myristoylated (1 μM). B, bar graph depicting quantification of evoked firing in the experimental conditions reported in A ($N = 5$ mice; $P = 0.072$; paired Student's t test; $n = 12$ cells). [Colour figure can be viewed at wileyonlinelibrary.com]

(Fig. 5C and B; number of APs: pre = 6.43 ± 1.94 ; post = 10.19 ± 2.54 ; $N = 4$ mice; $P = 0.018$; paired Student's t test; $n = 10$ cells), an effect that was prevented by prior application of the H2R antagonist ranitidine (Fig. 5E and B; number of APs: pre = 8.27 ± 0.88 ; post = 8.96 ± 1.44 ; $N = 5$ mice; $P = 0.298$; paired Student's t test; $n = 14$ cells).

Collectively, these findings suggest that histamine, through PKA-signalling, elicits long-lasting positive modulation of MSN excitability by acting at the H2R.

H2R activation affects sub- and suprathreshold conductances

It has been recently shown that PKA affects the excitability of striatal MSNs at subthreshold membrane potentials, thereby changing transitions to the up-state (Lahiri & Bevan, 2020). Therefore, to assess the impact of H2R-dependent signalling on MSNs undergoing down-to-up-state transitions, we first measured the first spike latency before and after dimaprit application. As shown in Fig. 6A and B, first spike latency was significantly reduced (first spike latency: pre = 357.21 ± 95.00 ms; post = 207.94 ± 83.00 ms; $N = 7$ mice; $P < 0.0001$; paired Student's t test; $n = 17$ cells). We then compared the MSN voltage trajectory during transitions from down-to-up-state before and after dimaprit application. Voltage responses to a suprathreshold current step before and after dimaprit application were superimposed and then subtracted to identify the appearance of H2R-sensitive components. These subtracted voltages were considered

to reflect divergent pre- and post-stimulus trajectories when they exceeded the mean plus 3 SDs of voltage differences in the 20 ms preceding current injection (Fig. 6E, right). According to this measure, differences in pre- and post-stimulus responses to current injection emerged at subthreshold voltages (Fig. 6E and B) that are consistent with negative modulation of K^+ conductances, such as the transient A-type K^+ currents (Kim et al., 2007; Mendonca et al., 2018) that, in MSNs of the NAc, are mainly carried by Kv4.2 channels (Aceto et al., 2020).

Kv4.2 channels underlie a fast A-type current that influences subthreshold excitability and firing in striatal MSNs (Carrillo-Reid et al., 2019; Tkatch et al., 2000). Although histaminergic modulation of Kv4.2 channels has not been reported in MSNs, PKA downregulates these channels in other cell types (Hoffman & Johnston, 1998). Furthermore, genetic deletion of Kv4.2 enhances striatal MSN excitability (Carrillo-Reid et al., 2019). Since Kv4.2 channels also mediate suprathreshold currents contributing to AP afterhyperpolarization (AHP) and AP half-width (Kim et al., 2005), we examined whether H2R activation affects these two AP parameters. Therefore, we measured medium AHP (mAHP) peak voltages before and after dimaprit application. As shown in Fig. 7A and B, we observed a significant reduction in mAHP after dimaprit application (mAHP amplitude: pre = 9.27 ± 1.33 mV; post = 7.49 ± 1.66 mV; $N = 7$ mice; $P = 0.0003$; paired Student's t test; $n = 17$ cells). Consistent with negative modulations of Kv4.2 channels, H2R activation also significantly increased the AP

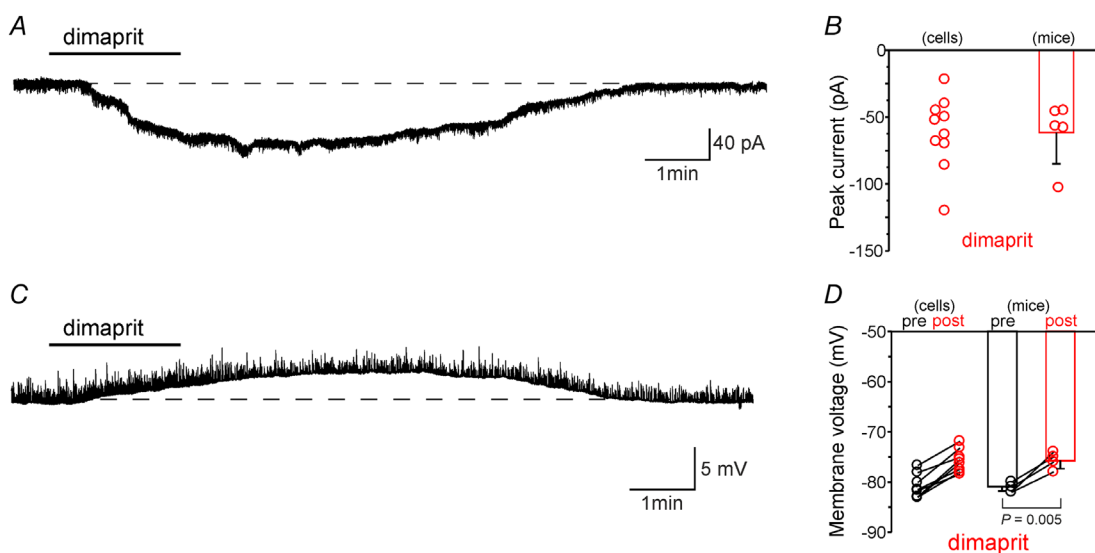


Figure 4. H2R activation induces tonic currents and mild depolarization in NAc MSNs

A, representative trace showing the inward current elicited by 10 μ M dimaprit. B, bar graph depicting quantification of dimaprit-induced inward currents ($N = 5$ mice; $n = 10$ cells). C, representative example of membrane depolarization induced by dimaprit. D, mean values of effects induced by dimaprit on membrane voltage ($N = 4$ mice; $P = 0.005$; paired Student's t test; $n = 8$ cells). [Colour figure can be viewed at wileyonlinelibrary.com]

half-width (dimaprit AP half-width: pre = 1.19 ± 0.29 ms; post = 1.30 ± 0.29 ms; $N = 7$ mice; $P = 0.010$; paired Student's t test; $n = 17$ cells; vehicle AP half-width: pre = 1.28 ± 0.23 ms; post = 1.27 ± 0.24 ms; $N = 3$ mice; $P = 0.260$; paired Student's t test; $n = 9$ cells; Fig. 7C and D).

Several ion channels, other than Kv4.2, have been proposed as targets of PKA-dependent modulation. They include voltage-dependent K^+ (Kv) channels, such as Kv1.2-containing channels (Shen et al., 2004) and voltage-dependent Na^+ (Na_v1) channels (Surmeier & Kitai, 1993).

Negative modulation of Kv1.2-containing channels may contribute to H2R-dependent elevation of MSN excitability. To test this possibility, we bath applied α -dendrotoxin (α -DTX; 100 nM) to inhibit

Kv1.2-containing channels for at least 10 min prior to dimaprit application. In the presence of α -DTX, dimaprit still increased MSN firing rate (number of APs: pre = 6.40 ± 1.05 ; post = 11.05 ± 1.98 ; $N = 3$ mice; $P = 0.015$; paired Student's t test; $n = 6$ cells; data not shown), thus suggesting that Kv1.2-containing channels are not involved in H2R-dependent elevation of MSN excitability.

PKA has been proposed to modulate Na_v1 channels in rat striatal neurons (Schiffmann et al., 1995), which should raise the threshold for firing and decrease the peak amplitude of Na^+ currents (Schiffmann et al., 1995; Surmeier & Kitai, 1993), thus limiting the elevation of firing. To examine the possible impact of Na_v1 channel modulation by H2R activation, we compared AP amplitudes and thresholds before and after dimaprit

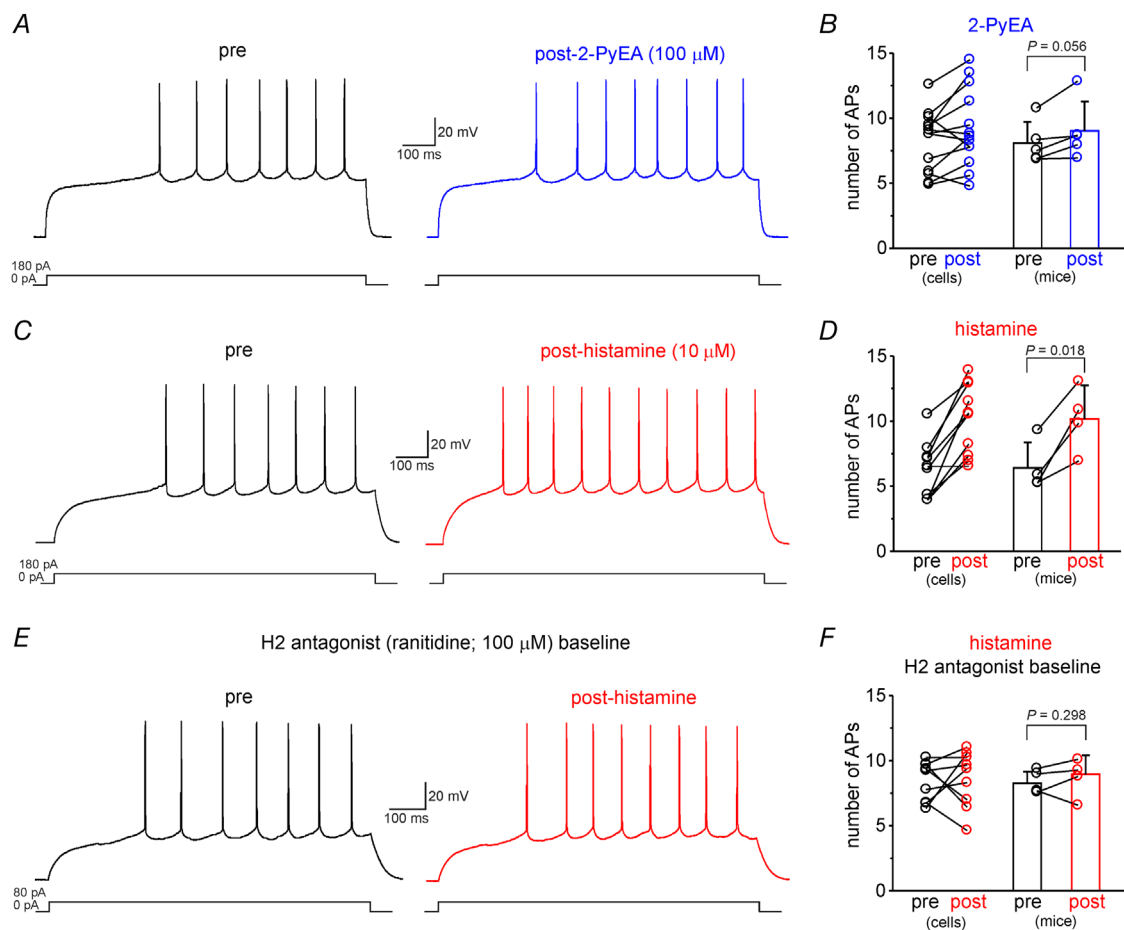


Figure 5. Pharmacological activation of H1R failed to affect the frequency of evoked firing in MSNs

A, representative traces showing current-evoked firing of an MSN before and after local perfusion of H1R agonist (2-PyEA; 100 μ M). B, normalized mean \pm SD for $N = 5$ mice in which 2-PyEA was applied ($P = 0.056$; paired Student's t test; $n = 13$ cells). C and D, representative traces (C) and summary plot (D) illustrating that histamine application increased evoked firing ($N = 4$ mice; $P = 0.019$; paired Student's t test; $n = 10$ cells). E, representative traces showing that histamine-dependent modulation of evoked firing was not observed when slices were pre-incubated (5–20 min) with the H2R antagonist ranitidine (100 μ M). F, bar graph depicting quantification of evoked firing in the experimental conditions reported in E ($N = 5$ mice; $P = 0.298$; paired Student's t test; $n = 14$ cells). [Colour figure can be viewed at wileyonlinelibrary.com]

application. Threshold values were determined from AP waveform averages by detecting the first point of sustained positive acceleration (second derivative) of voltage, as described previously (Baufreton et al., 2005). Using this method, we observed no significant differences in AP threshold following H2R activation (pre = -41.87 ± 5.40 mV; post = -41.77 ± 4.92 mV; $N = 7$ mice; $P = 0.818$; paired Student's t test; $n = 17$ cells; Fig. 7E). However, AP amplitude was significantly decreased (dimaprit AP amplitude: pre = 72.35 ± 2.72 mV; post = 69.07 ± 2.09 mV; $N = 7$ mice; $P = 0.004$; paired Student's t test; $n = 17$ cells; vehicle AP amplitude: pre = 68.38 ± 1.50 mV; post = 67.85 ± 1.37 mV; $N = 4$ mice; $P = 0.117$; paired Student's t test; $n = 9$ cells; Fig. 7F and G). While this observation indicates negative modulation of Na_v channels, it appears not to be sufficient to counteract the elevation of firing induced by H2R activation.

H2R stimulation increases evoked firing through reduced Kv4.2-mediated currents

The data shown so far suggest that negative modulation of Kv4.2 channels may underlie H2R-induced increases in evoked firing. To corroborate these findings, we performed a new set of experiments in which the effect of dimaprit on MSN-evoked firing was studied in the presence of the specific Kv4 channel blocker, AmmTX3. We hypothesized that if the H2R-dependent increase in evoked firing was due to reduced Kv4.2 channel activity, the pharmacological blockade of these channels would attenuate the effect of dimaprit. We first examined the effects of the pharmacological A-type K^+ current blockade on evoked firing. As shown in Fig. 8A and B, when 200 nM AmmTX3 was locally applied, the firing was significantly increased (number of APs: pre = 6.50 ± 0.75 ; post = 11.20 ± 1.11 ; $N = 4$ mice; $P = 0.001$; paired Student's t test; $n = 9$ cells). It is noteworthy that at this

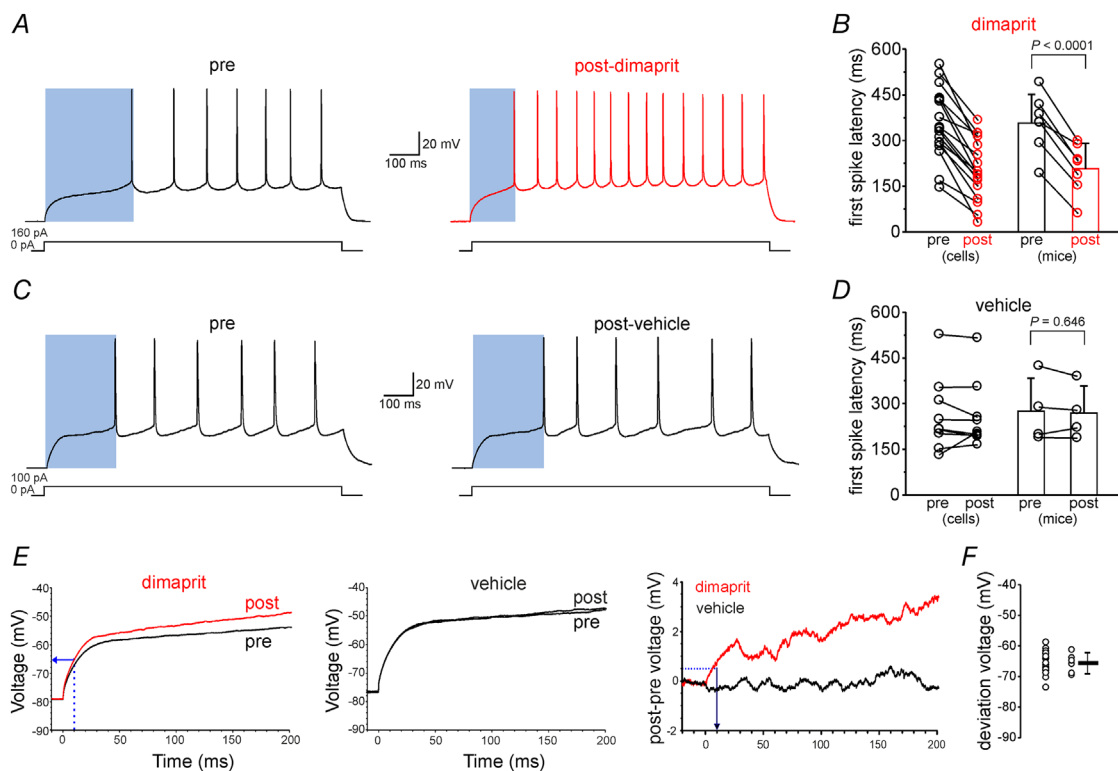


Figure 6. H2R activation reduces first spike latency and increases voltage responses at subthreshold voltages

A, representative traces showing reduced first spike latency following local dimaprit perfusion. B, summary plot of the reduced first spike latency shown in A ($N = 7$ mice; $P < 0.0001$; paired Student's t test; $n = 17$ cells). C and D, representative traces (C) and bar graph (D) of control experiments showing that first spike latency was not affected by local vehicle perfusion ($N = 4$ mice; $P = 0.647$; $n = 9$ cells). E, following dimaprit perfusion, responses to suprathreshold current injection were amplified at subthreshold voltages. E, left: deviation voltage (arrow; blue) was determined from the post-stimulus trajectory at the time of its divergence from the pre-stimulus trajectory (blue, dashed). E, right: time of voltage deviation (blue, arrow) was determined from the plot of voltage differences as described in the Results (blue, dashed) and was not apparent following vehicle perfusion (E, middle). F, bar graph showing the mean value of the deviation voltages (-65.8 ± 3.14 mV; $N = 6$ mice; $n = 17$ cells). [Colour figure can be viewed at wileyonlinelibrary.com]

concentration AmmTX3 reduced the A-type K^+ current amplitudes by about 40% (Maffie et al., 2013; Pathak et al., 2016), a level that still allows cell firing. Interestingly, the magnitude of the increased evoked firing by AmmTX3 was similar to that observed when dimaprit was applied (Fig. 2). Of note, AmmTX3 also mimicked dimaprit's effects on first spike latency, mAHP, half-width and voltage responses at subthreshold voltages (Fig. 9A and B; first spike latency: pre = 363.48 ± 103.12 ms; post = 232.00 ± 87.09 ms; $N = 4$ mice; $P = 0.003$; paired Student's t test $n = 9$ cells; Fig. 9F and B; mAHP amplitude: pre = -7.91 ± 1.48 mV; post: -7.05 ± 1.66 mV; $N = 4$ mice; $P = 0.019$; paired Student's t test; $n = 9$ cells; AP half-width: pre = 1.30 ± 0.39 ms; post = 1.46 ± 0.37 ms; $N = 4$ mice; $P = 0.020$; paired Student's t test; $n = 9$ cells; Fig. 9C and B; average deviation voltage = -62.40 ± 4.44 mV; $N = 4$ mice; $n = 11$ cells).

We then performed occlusion experiments by recording evoked firing before and after dimaprit application in brain slices perfused with AmmTX3. Consistently, under these experimental conditions, evoked firing was not significantly increased by H2R activation (number of APs: pre = 7.28 ± 1.42 ; post = 7.55 ± 1.30 ; $N = 5$ mice; $P = 0.092$; paired Student's t test; $n = 10$ cells; Fig. 8C and B). These findings supported our hypothesis that increased H2R-induced firing relies on down-regulation of $Kv4.2$ channels.

We next performed whole-cell patch-clamp recordings in voltage-clamp configuration and compared the magnitude of A-type K^+ currents before and after H2R activation. In NAc MSNs, whole-cell voltage-clamp recordings of the total outward currents in response to voltage steps ranging from -110 to $+40$ mV revealed an early A-type K^+ current, which could be isolated by

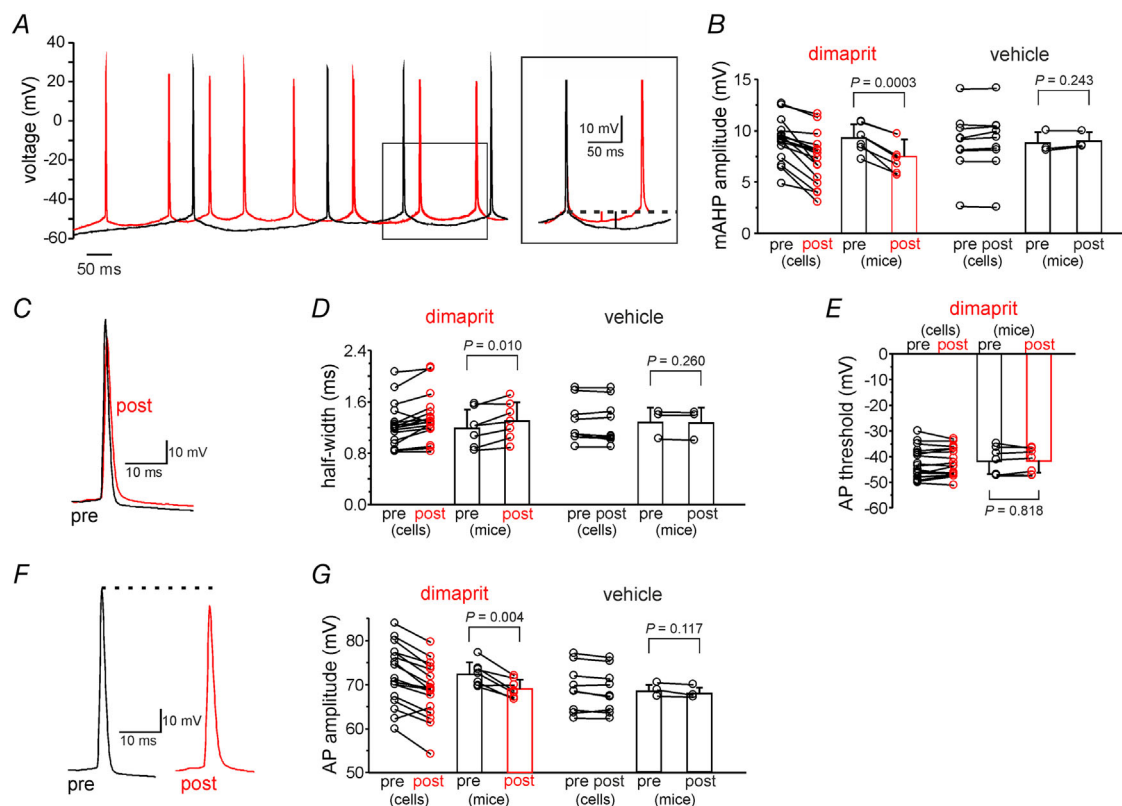


Figure 7. H2R activation affects mAHP amplitude, half-width and AP amplitude without changing AP threshold

A, representative traces showing reduced mAHP following dimaprit application. B, bar graph depicting quantification of mAHP amplitude in the experimental conditions showed in A ($N = 7$ mice; $P = 0.0003$; paired Student's t test; $n = 17$ cells). Quantification of mAHP amplitude before and after vehicle application is also shown (pre = 8.76 ± 1.06 mV; post = 8.97 ± 0.84 mV; $N = 3$ mice; $P = 0.243$; paired Student's t test; $n = 9$ cells). C, superimposition of APs highlighting decreased mAHP amplitude and broadened AP following dimaprit application. D, summary plot showing mean values of AP half-width before and after dimaprit ($N = 7$ mice; $P = 0.010$; paired Student's t test; $n = 17$ cells) and vehicle perfusion ($N = 3$ mice; $P = 0.260$; paired Student's t test; $n = 9$ cells). E and F, representative traces (E) and bar graph (F) showing reduced AP amplitude after dimaprit ($N = 7$ mice; $P = 0.004$; paired Student's t test; $n = 17$ cells) and vehicle perfusion ($N = 4$ mice; $P = 0.117$; paired Student's t test; $n = 9$ cells). G, summary plot illustrating that dimaprit perfusion had no effect on AP threshold ($N = 7$ mice; $P = 0.818$; paired Student's t test; $n = 17$ cells). [Colour figure can be viewed at wileyonlinelibrary.com]

applying a prepulse protocol (see Materials and Methods) in the presence of 20 mM TEA to suppress slower K⁺ currents (Aceto et al., 2020).

Under these experimental conditions we found that A-type K⁺ current amplitudes were significantly reduced by dimaprit application (pre = 2.85 ± 0.55 nA; post = 2.13 ± 0.41 nA; $N = 5$ mice; $P = 0.007$; paired Student's *t* test; $n = 12$ cells; Fig. 10A and B). Specifically, dimaprit induced a significantly more depolarized activation voltage ($V_{1/2}$: pre = -19.03 ± 8.14 mV; post = -10.62 ± 5.32 mV; $N = 5$ mice; $P = 0.013$; paired Student's *t* test; $n = 12$ cells; Fig. 10C and B), whereas the inactivation curve was not significantly shifted ($V_{1/2}$: pre = -40.43 ± 1.92 mV; post = 39.17 ± 1.81 mV; $N = 5$ mice; $P = 0.343$; paired Student's *t* test; Fig. 10E and B; $n = 12$ cells). Of note, when dimaprit was applied to MSNs that had been incubated with PKI ($1 \mu\text{M}$ for at least 10 min), no changes in A-type K⁺ current amplitudes were detected (pre = 1.98 ± 0.28 nA; post = 1.91 ± 0.40 nA; $N = 4$ mice; $P = 0.318$; paired Student's *t* test; $n = 10$ cells; Fig. 10B), indicating that H2R-induced negative modulation of Kv4.2, similarly to the positive modulation of evoked firing, requires PKA signalling.

These findings are in line with previous studies showing that PKA downregulates Kv4.2-mediated currents by directly phosphorylating the α -subunit, an effect that leads to changes in channel properties and internalization

(Hammond et al., 2008; Kim et al., 2007). Therefore, we asked whether H2R activation in MSNs may result in PKA-mediated Kv4.2 channel internalization. We first sought to test if H2R and Kv4.2 channels are co-expressed in MSNs. For this, we performed a new set of single-cell qRT-ddPCR experiments and found that the vast majority of screened MSNs (8 out of 9; $N = 4$ mice) expressed both H2R and Kv4.2 transcripts (Fig. 10F). To determine the membrane distribution of Kv4.2 channels after incubation of slices with dimaprit ($10 \mu\text{M}$; for 30 min), tissues were lysed, separated into membrane and cytoplasmic fractions, and analysed by western blotting. As shown in Fig. 10G and B, in slices incubated with dimaprit the levels of Kv4.2 protein were decreased in the membrane fraction, whereas the cytoplasmic fraction of the protein was increased. These results indicate that membrane localization of Kv4.2 is decreased following activation of H2R signalling.

Discussion

Here we report a novel mechanism by which H2R-dependent downregulation of Kv4.2 channels increases MSN excitability in the NAc through the PKA signalling pathway. This conclusion is supported by the following experimental evidence: (1) pharmacological activation of H2R results in increased evoked firing

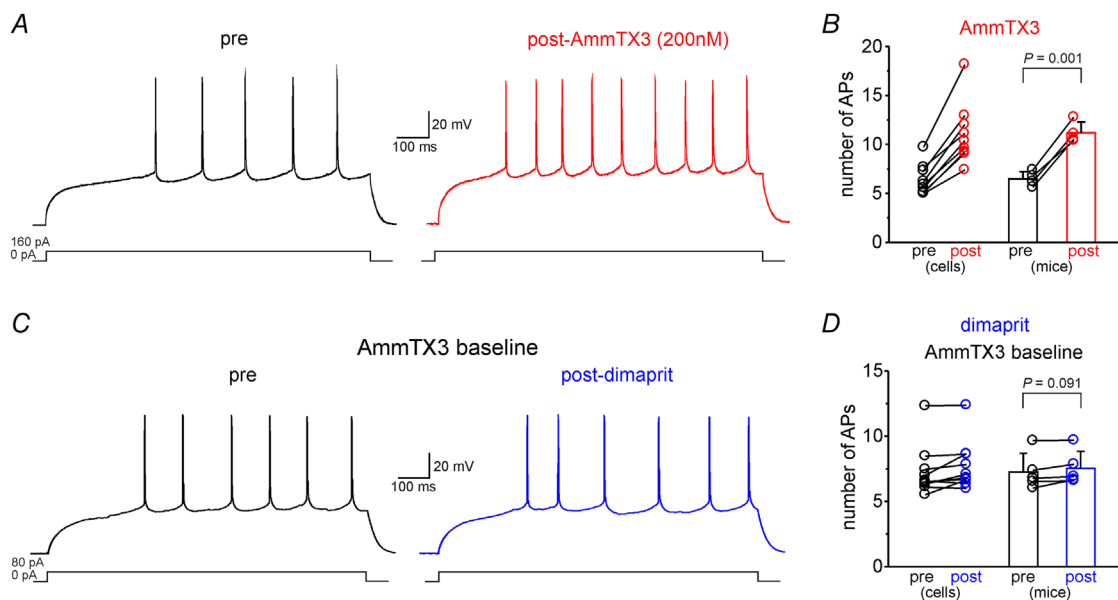


Figure 8. Pharmacological inhibition of Kv4.2 channels mimics and occludes dimaprit's effect on evoked firing

A, representative traces showing current-evoked firing in an MSN before (black) and after (red) local perfusion of the Kv4.2 channel inhibitor AmmTX3 (200 nM). B, bar graph showing mean AP number in which AmmTX3 was applied ($N = 4$ mice; $P = 0.001$; paired Student's *t* test; $n = 9$ cells). C, representative traces showing that the presence of AmmTX3 in the bath prevented the increase of the evoked firing induced by dimaprit application. D, summary plot illustrating quantification of the evoked firing in the experimental conditions reported in C ($N = 5$ mice; $P = 0.092$; paired Student's *t* test; $n = 10$ cells). [Colour figure can be viewed at wileyonlinelibrary.com]

and A-type current down-regulation; (2) increased H2R-induced firing is prevented by pharmacological inhibition of PKA signalling; (3) blockade of A-type K^+ currents mimics and occludes the H2R-induced effect on excitability; and (4) the H2R signalling pathway decreases surface expression of Kv4.2 channels.

H2Rs are abundantly expressed in the NAc (Takagi et al., 1986; Shoblock & O'Donnell, 2000). Our results from single-cell ddPCR experiments confirmed the expression of H2R and H1R in MSNs of the NAc and indicated that H2R is the prevailing postsynaptic HA receptor expressed in the NAc. Although MSNs of the NAc are typically classified as dopamine D1 receptor and dopamine D2 receptor subtypes, which belong to the

direct and indirect pathway (Kupchik et al., 2015), we speculate that H2R is expressed independently in the two MSN subpopulations as the majority of the MSNs tested (18 out of 20) expressed mRNA for H2R.

H2R-dependent effects on neuronal properties and/or ion channels have been the object of several studies, and it is generally believed that activation of H2R signalling has an excitatory effect in the CNS (Haas & Panula, 2003; Haas et al., 2008; Panula & Nuutinen, 2013; Panula et al., 2015). In particular, activation of H2R leads to: (1) block of a Ca^{2+} -activated potassium conductance (small K) responsible for the accommodation of firing and the long-lasting afterhyperpolarization following APs in pyramidal cells (Pedarzani & Storm, 1993);

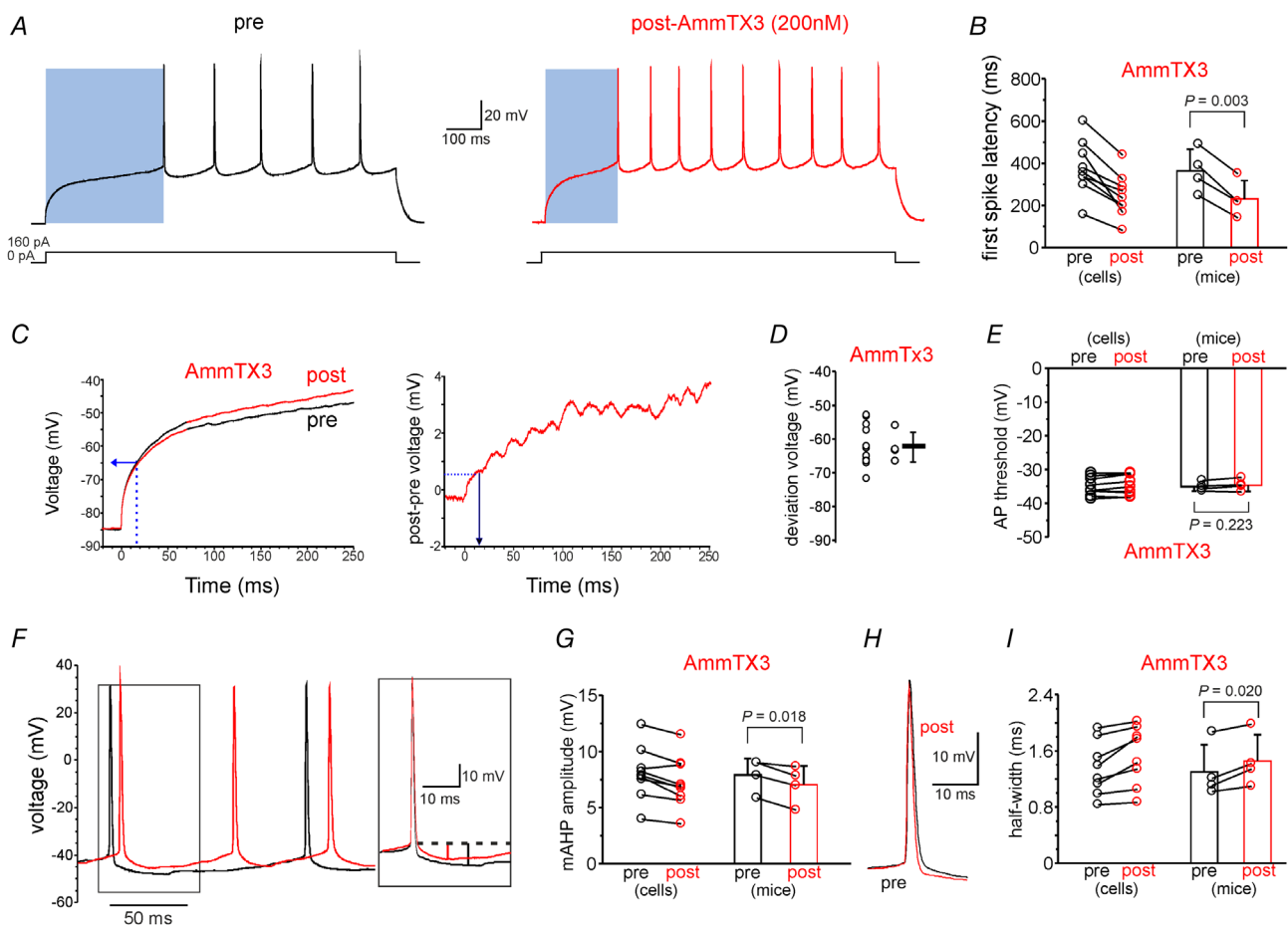


Figure 9. Pharmacological Kv4.2 channel inhibition mimics the effects of dimaprit on first spike latency, voltage responses at subthreshold voltages, mAHP amplitude and half-width

A, representative traces showing reduced first spike latency following local AmmTX3 perfusion. **B**, summary plot of the reduced first spike latency shown in **A** ($N = 4$; $P = 0.003$; paired Student's t test; $n = 9$ cells). **C** and **D**, following AmmTX3 perfusion, responses to suprathreshold current injection were similar to that induced by dimaprit (see Fig. 5 for comparison). **E**, summary plot illustrating that AmmTX3 perfusion had no effect on AP threshold ($N = 4$ mice; $P = 0.223$; paired Student's t test; $n = 9$ cells). **F**, representative traces showing reduced mAHP following AmmTX3 application. **G**, bar graph depicting quantification of mAHP amplitude in the experimental conditions showed in **F** ($N = 4$ mice; $P = 0.018$; paired Student's t test; $n = 9$ cells). **H**, superimposition of APs before and after AmmTX3 application demonstrating significantly decreased AP half-width amplitude. **I**, summary plot showing mean values of AP half-width ($N = 4$ mice; $P = 0.020$; paired Student's t test; $n = 9$ cells). [Colour figure can be viewed at wileyonlinelibrary.com]

(2) depolarization of pyramidal and thalamic neurons via a direct action of cAMP on the hyperpolarization-activated cation channels (McCormick & Williamson, 1991); (3) membrane depolarization via blockade of a leak potassium conductance in dissociated striatal cholinergic interneurons (Munakata & Akaïke, 1994); (4) membrane depolarization of striatal MSNs (Zhuang et al., 2018); and (5) reduction of A-type K^+ currents responsible for the elevation of excitability during both slow synaptic excitation and slow synaptic

excitation-like responses in myenteric neurons (Starodub & Wood, 2000). On the other hand, the maximum firing frequency of fast-spiking hippocampal interneurons is reduced through H2R activation, PKA and blockade of Kv3.2 channels (Atzori et al., 2000).

Although these studies indicate that H2R activation may modulate multiple ion channels, in NAc MSNs we found that only Kv4.2-containing channels are targeted by H2R downstream signalling. Indeed, the acceleration of MSN down- to up-state transitions and increased

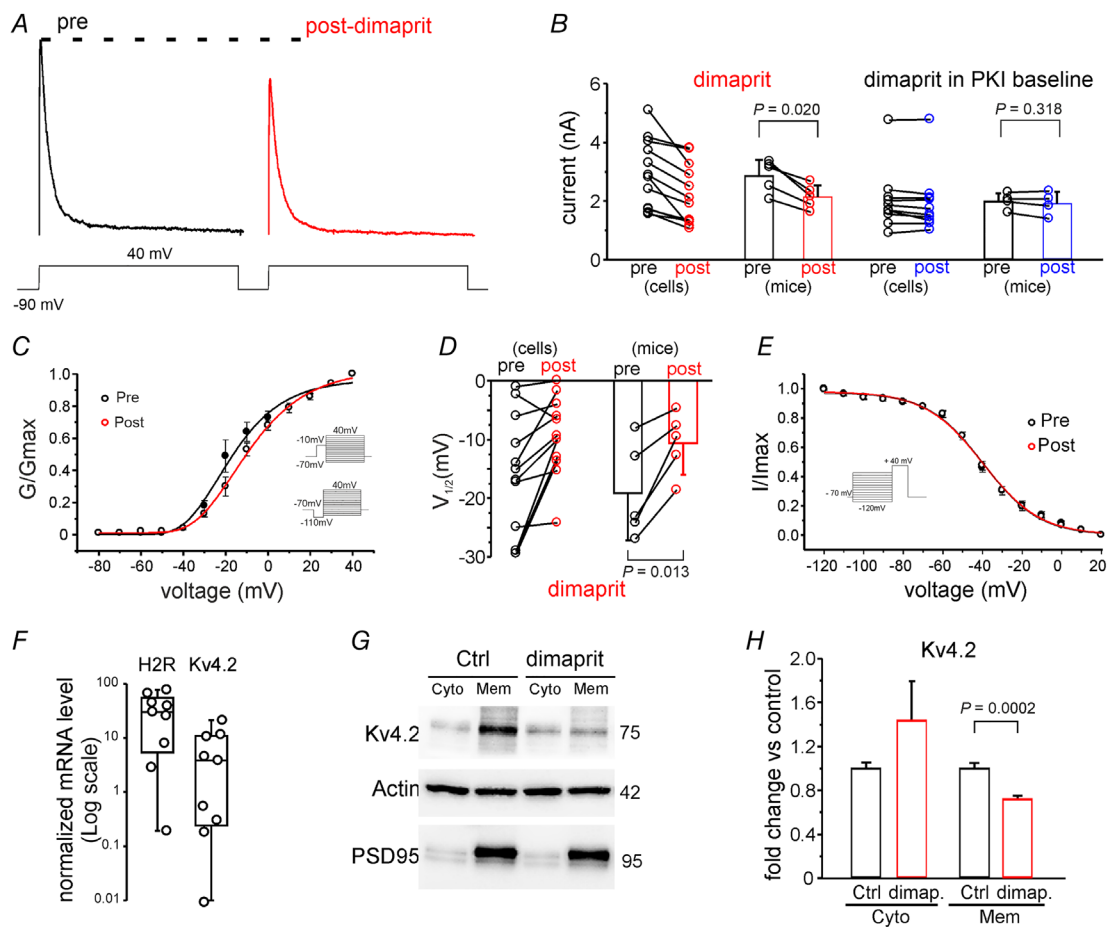


Figure 10. Pharmacological activation of H2R reduces A-type K^+ currents

A, representative traces showing transient A-type K^+ currents recorded in MSNs before (black) and after (red) dimaprit application. B, summary plot showing the decreased A-type K^+ currents induced by dimaprit ($N = 5$ mice; $P = 0.007$; paired Student's t test; $n = 12$ cells). Note that when PKI was present in the bath, A-type K^+ currents were not significantly decreased by dimaprit ($N = 4$ mice; $P = 0.318$; paired Student's t test; $n = 10$ cells). C, activation curve showing the normalized A-type K^+ current conductance before and after dimaprit application. Note that the activation curve is shifted toward more depolarized membrane potential after dimaprit application. D, bar graph showing mean \pm SD voltage at which half of the current was activated ($V_{1/2}$ acquired from a Boltzmann fit of the curve). The mean $V_{1/2}$ measured after dimaprit application was significantly different from that recorded before application ($N = 5$ mice; $P = 0.038$; paired Student's t test; $n = 12$ cells). G, conductance; G_{max} , maximum G. E, steady-state inactivation curves in control and after dimaprit application. F, box plot showing H2R and Kv4.2 mRNA levels by ddPCR in single NAc MSNs ($N = 4$ mice; $n = 9$ cells). G, representative Western blots of NAc tissues showing levels of membrane and cytosolic fractions of Kv4.2 in control slices and slices incubated with dimaprit. H, densitometry analysis for the blots probed with anti Kv4.2 channels and normalized to actin. PSD95 immunoreactivity was used as an internal control of membrane-bound protein, which was not modulated by dimaprit ($N = 6$ mice; statistics by ANOVA with Bonferroni's *post hoc* test; $P = 0.0002$). [Colour figure can be viewed at wileyonlinelibrary.com]

firing frequency are consistent with downregulation of Kv4.2-containing channels (Carrillo-Reid et al., 2019; Tkatch et al., 2000). Kv4.2 is the primary pore-forming Kv channel subunit underlying the rapidly activating and inactivating somatodendritic A-type K^+ current in MSNs of the NAc (Aceto et al., 2020). Operating at sub- and suprathreshold voltages, Kv4.2 has been reported to regulate AP repolarization and repetitive firing (Johnston et al., 2000). Moreover, it is well known that among the different channels contributing to AP kinetics, A-type K^+ channels contribute to AHP and AP duration (Kim et al., 2005; Storm, 1987; Zhang & McBain, 1995). Neurons with decreased A-type channel expression would have shorter AHP amplitudes and AP broadening, which are features allowing neurons to have higher AP firing frequency (Carrasquillo et al., 2012; Kim et al., 2005). Consistently, in our study all these effects were found in MSNs after H2R activation and following pharmacological blockade of A-type K^+ currents. Furthermore, our finding that H2R activation reduces A-type K^+ currents in MSNs, together with the evidence that the pharmacological blockade of A-type K^+ currents occludes the H2R-induced increase in MSN excitability, strongly supports the conclusion that the Kv4.2 channel is a downstream target of H2R signalling in NAc MSNs.

In contrast to the ion channel target described above, we did not find evidence for significant involvement of Kv1.2 and Nav1 channels in the H2R-dependent modulation of MSN excitability. Downregulation of Kv1.2 has been proposed to underlie the PKA-dependent increase in evoked discharge of striatal MSNs (Lahiri & Bevan, 2020). However, DTX, the selective Kv1.2 channel inhibitor, failed to prevent the H2R-induced increase of evoked firing, suggesting that these K^+ channels are not targets of the H2R signalling pathways. With regard to Nav1 modulation, in agreement with previous studies reporting PKA-dependent downregulation of Nav1 channels (Cantrell et al., 1999; Few et al., 2007), we found a reduction of AP amplitude following H2R activation. This effect should inhibit down- to up-state transitions. However, we found that the transition to up-state firing was enhanced while the AP threshold was unaffected by H2R activation. One possible explanation for these findings is that H2R modulation of Nav1.2 is not sufficient to oppose the elevated firing induced by downregulation of Kv4.2 channels.

A-type K^+ currents are essential for the proper functioning of neurons, where they act as key regulators in AP repolarization, repetitive firing and back-propagation of APs (Norris & Nerbonne, 2010; Yuan et al., 2005). In addition, the gating properties and distribution of A-type K^+ channels influence the intracellular Ca^{2+} levels in dendritic branches (Chen et al., 2006). Because Ca^{2+} is fundamental to many forms of synaptic plasticity in dendrites, the regulatory effects of A-type K^+ channels

on dendritic excitability are consequentially critical for dendritic and synaptic processing during synaptic plasticity (Chen et al., 2006). Although A-type K^+ currents are critical for neuronal functions in almost all brain structures, only recently has the molecular identity of these currents been elucidated in MSNs of the NAc (Aceto et al., 2020). In this study, beyond the demonstration that A-type K^+ currents are primarily mediated by Kv4.2 channels, a Kv4.2-dependent molecular mechanism of MSN maladaptive plasticity underlying depressive-like behaviours in mice (Aceto et al., 2020) has been identified. To our knowledge, this is the only study reporting a pathophysiological role for Kv4.2 in the NAc, which has been implicated in numerous neurological and psychiatric disorders, including depression, anxiety disorders, obsessive-compulsive disorder, Parkinson's disease, Alzheimer's disease, obesity, and in drug misuse and addiction (Salgado & Kaplitt, 2015). Considering the fundamental role of Kv4.2 in neuronal excitability and synaptic plasticity, it is tempting to speculate that Kv4.2 dysregulation may play a role in different neurological and psychiatric disorders involving maladaptive plasticity and excitability of NAc MSNs.

Different studies have shown complex phosphorylation-dependent regulation of Kv4.2 with functional consequences for transient A-type K^+ currents (Anderson et al., 2000). *In vitro* phosphorylation of recombinant fragments of Kv4.2 revealed PKA-mediated phosphorylation of Kv4.2 (Anderson et al., 2000). It is noteworthy that PKA-mediated phosphorylation leads to decreased Kv4.2 current and that PKA directly phosphorylates Kv4.2 at S552 (Hammond et al., 2008). In particular, activation of PKA leads to a change in the voltage-dependent activation of Kv4.2 channels, causing a rightward shift in the activation curve (Hoffman & Johnston, 1998). In addition to the regulation of Kv4.2 channel properties, it has been proposed that S552 is a regulatory site inducing activity-dependent internalization of Kv4.2 in neuronal dendrites (Hammond et al., 2008; Kim et al., 2007). In particular, PKA activation with forskolin induces Kv4.2 internalization from dendritic spines, whereas PKA inhibition with H89 prevented this effect in hippocampal neurons (Hammond et al., 2008). Importantly, the same study also showed that a point mutation at the C-terminal PKA phosphorylation site of Kv4.2 (Serine 552) prevented the channel internalization. PKA-mediated phosphorylation at S552 also enhanced surface expression of Kv4.2 induced by interaction with cytoplasmic K^+ channel-interacting protein auxiliary subunits (KCHIP4a), an effect that requires phosphorylation at S552 (Lin et al., 2010). Moreover, a role for Kv4.2 trafficking is also played by A-kinase anchoring proteins (AKAPs) that associate with Kv4.2, enhancing expression of the Kv4.2/ KCHIP4a complex (Lin et al., 2010). Together, these findings

suggest that Kv4.2 channels form a membrane-bound pool of macromolecular complexes whose activity end expression can be regulated by PKA through AKAP interaction. In line with the above evidence, we found that activation of H2R signalling, in addition to regulating Kv4.2 channel properties, induces channel internalization in NAc MSNs. The anti-Kv4.2/KCND2 phospho-Ser-552 antibody is not commercially available and, therefore, it remains to be verified whether activation of H2R signalling results in increased phosphorylation levels at the S552 site of the Kv4.2 channel.

In agreement with previous studies (Ellender et al., 2011; Zhuang et al., 2018), we also show that H2R activation causes membrane depolarization of MSNs, probably through activation of a subthreshold conductance (Haas & Panula, 2003). Although this effect may contribute to MSN excitability, it is not responsible for the enhanced spike firing we reported because this effect was recorded after injection of hyperpolarized currents compensating for membrane potential changes.

In the present study, H1R activation failed to significantly affect evoked firing in MSNs. Low levels of H1R expression may account for the lack of effect we observed. However, we cannot exclude the possibility of a greater sensitivity of H1R signalling to washout of intracellular factors during whole-cell patch-clamp recordings (Horn & Marty, 1988). In this regard, a recent elegant study by Lahiri & Bevan (2020) demonstrated that whole-cell recordings of MSNs can lead to significant dialysis of cytosolic components altering their response to dopaminergic signalling.

The H1R is linked to an intracellular G-protein ($G\alpha q/11$) that activates the phospholipase C- β (PLC β) signalling pathway. Typically, H1R activation excites neurons in most brain regions, including the thalamus (McCormick & Williamson, 1991; Soria-Jasso et al., 1997; Zhou et al., 2006), amygdala, septum (Gorelova & Reiner, 1996; Xu et al., 2004), hippocampus (Selbach et al., 1997) and striatum (Zhuang et al., 2018).

With regard to the potential implications of our findings within the context of the pathophysiological role of histaminergic system in the CNS, it is noteworthy that the NAc is a pivotal node in the limbic basal ganglia loop, and its dysfunction may result in psychiatric diseases including stress-related disorders such as depression, anxiety and addiction (Francis & Lobo, 2017; Gunaydin & Kreitzer, 2016). Indeed, accumulating experimental and clinical evidence indicates that the NAc holds a key position in motivation, emotion and cognition, and is strongly implicated in the psychopathology and treatment of stress-related disorders (Bagot et al., 2015; Christoffel et al., 2015). Interestingly, increases in HA-containing TMN neuron output during behavioural states heightened awareness of salient environmental stimuli including acute stress, fear learning and systemic metabolic restraint

(Ito, 2000; Manz et al., 2021; Miklos & Kovacs, 2003; Taylor & Snyder, 1971). In this context, it has been recently reported that stress-evoked HA signalling recruits a presynaptic gain control mechanism at glutamatergic synapses in the NAc, an effect that is mediated by H3R (Manz et al., 2021). Moreover, it has been demonstrated that activation of the histaminergic afferent system, particularly the histamine H3R, inhibits glutamatergic synaptic transmission in the circuit from the pre-limbic prefrontal cortex to the NAc and improves both anxiety- and obsessive-compulsive-like behaviours induced by restraint stress (Zhang et al., 2020). The H2R-dependent enhancement of MSN excitability we observed in this study could conceivably represent another mechanism by which elevated extracellular histamine levels, following acute stress, may induce stress-dependent decisional strategies. Therefore, our findings encourage further studies aimed at elucidating the role of NAc H2R in stress-associated physiological states. Given the well-characterized role of the NAc in goal-directed behaviours, it is tempting to speculate that H2R signalling gates stress-induced MSN adaptation.

References

- Aceto, G., Colussi, C., Leone, L., Fusco, S., Rinaudo, M., Scala, F., Green, T. A., Laezza, F., D'Ascenzo, M., & Grassi, C. (2020). Chronic mild stress alters synaptic plasticity in the nucleus accumbens through GSK3 β -dependent modulation of Kv4.2 channels. *Proc Natl Acad Sci U S A*, **117**, 8143–8153.
- Anderson, A. E., Adams, J. P., Qian, Y., Cook, R. G., Pfaffinger, P. J., & Sweatt, J. D. (2000). Kv4.2 phosphorylation by cyclic AMP-dependent protein kinase. *Journal of Biological Chemistry*, **275**, 5337–5346.
- Atzori, M., Lau, D., Tansey, E. P., Chow, A., Ozaita, A., Rudy, B., & McBain, C. J. (2000). H2 histamine receptor-phosphorylation of Kv3.2 modulates interneuron fast spiking. *Nature Neuroscience*, **3**, 791–798.
- Bagot, R. C., Parise, E. M., Pena, C. J., Zhang, H. X., Maze, I., Chaudhury, D., Persaud, B., Cacho, R., Bolanos-Guzman, C. A., Cheer, J. F., Deisseroth, K., Han, M. H., & Nestler, E. J. (2015). Ventral hippocampal afferents to the nucleus accumbens regulate susceptibility to depression. *Nature Communication*, **6**, 7062.
- Baufreton, J., Atherton, J. F., Surmeier, D. J., & Bevan, M. D. (2005). Enhancement of excitatory synaptic integration by GABAergic inhibition in the subthalamic nucleus. *Journal of Neuroscience*, **25**, 8505–8517.
- Bromberg-Martin, E. S., Matsumoto, M., & Hikosaka, O. (2010). Dopamine in motivational control: Rewarding, aversive, and alerting. *Neuron*, **68**, 815–834.
- Cadwell, C. R., Palasantza, A., Jiang, X., Berens, P., Deng, Q., Yilmaz, M., Reimer, J., Shen, S., Bethge, M., Tolias, K. F., Sandberg, R., & Tolias, A. S. (2016). Electrophysiological, transcriptomic and morphologic profiling of single neurons using Patch-seq. *Nature Biotechnology*, **34**, 199–203.

- Cadwell, C. R., Scala, F., Li, S., Livrizzi, G., Shen, S., Sandberg, R., Jiang, X., & Tolias, A. S. (2017). Multimodal profiling of single-cell morphology, electrophysiology, and gene expression using Patch-seq. *Nature Protocols*, **12**, 2531–2553.
- Cantrell, A. R., Tibbs, V. C., Westenbroek, R. E., Scheuer, T., & Catterall, W. A. (1999). Dopaminergic modulation of voltage-gated Na⁺ current in rat hippocampal neurons requires anchoring of cAMP-dependent protein kinase. *Journal of Neuroscience*, **19**, RC21.
- Carrasquillo, Y., Burkhalter, A., & Nerbonne, J. M. (2012). A-type K⁺ channels encoded by Kv4.2, Kv4.3 and Kv1.4 differentially regulate intrinsic excitability of cortical pyramidal neurons. *Journal of Physiology*, **590**, 3877–3890.
- Carrillo-Reid, L., Day, M., Xie, Z., Melendez, A. E., Kondapalli, J., Plotkin, J. L., Wokosin, D. L., Chen, Y., Kress, G. J., Kaplitt, M., Ilijic, E., Guzman, J. N., Chan, C. S., & Surmeier, D. J. (2019). Mutant huntingtin enhances activation of dendritic Kv4 K(+) channels in striatal spiny projection neurons. *Elife*, **8**, e40818.
- Chen, X., Yuan, L. L., Zhao, C., Birnbaum, S. G., Frick, A., Jung, W. E., Schwarz, T. L., Sweatt, J. D., & Johnston, D. (2006). Deletion of Kv4.2 gene eliminates dendritic A-type K⁺ current and enhances induction of long-term potentiation in hippocampal CA1 pyramidal neurons. *Journal of Neuroscience*, **26**, 12143–12151.
- Christoffel, D. J., Golden, S. A., Walsh, J. J., Guise, K. G., Heshmati, M., Friedman, A. K., Dey, A., Smith, M., Rebusi, N., Pfau, M., Ables, J. L., Aleyasin, H., Khibnik, L. A., Hodes, G. E., Ben-Dor, G. A., Deisseroth, K., Shapiro, M. L., Malenka, R. C., Ibanez-Tallon, I., ... Russo, S. J. (2015). Excitatory transmission at thalamo-striatal synapses mediates susceptibility to social stress. *Nature Neuroscience*, **18**, 962–964.
- Dolen, G., Darvishzadeh, A., Huang, K. W., & Malenka, R. C. (2013). Social reward requires coordinated activity of nucleus accumbens oxytocin and serotonin. *Nature*, **501**, 179–184.
- Ellenbroek, B. A., & Ghiabi, B. (2014). The other side of the histamine H3 receptor. *Trends in Neuroscience (Tins)*, **37**, 191–199.
- Ellender, T. J., Huerta-Ocampo, I., Deisseroth, K., Capogna, M., & Bolam, J. P. (2011). Differential modulation of excitatory and inhibitory striatal synaptic transmission by histamine. *Journal of Neuroscience*, **31**, 15340–15351.
- Few, W. P., Scheuer, T., & Catterall, W. A. (2007). Dopamine modulation of neuronal Na(+) channels requires binding of A kinase-anchoring protein 15 and PKA by a modified leucine zipper motif. *Proc Natl Acad Sci U S A*, **104**, 5187–5192.
- Francis, T. C., & Lobo, M. K. (2017). Emerging role for nucleus accumbens medium spiny neuron subtypes in depression. *Biological Psychiatry*, **81**, 645–653.
- Gervasi, N., Hepp, R., Tricoire, L., Zhang, J., Lambolez, B., Paupardin-Tritsch, D., & Vincent, P. (2007). Dynamics of protein kinase A signaling at the membrane, in the cytosol, and in the nucleus of neurons in mouse brain slices. *Journal of Neuroscience*, **27**, 2744–2750.
- Gorelova, N., & Reiner, P. B. (1996). Histamine depolarizes cholinergic septal neurons. *Journal of Neurophysiology*, **75**, 707–714.
- Groenewegen, H. J., Wright, C. I., Beijer, A. V., & Voorn, P. (1999). Convergence and segregation of ventral striatal inputs and outputs. *Annals of the New York Academy of Sciences*, **877**, 49–63.
- Gunaydin, L. A., & Kreitzer, A. C. (2016). Cortico-basal ganglia circuit function in psychiatric disease. *Annual Review of Physiology*, **78**, 327–350.
- Haas, H., & Panula, P. (2003). The role of histamine and the tuberomammillary nucleus in the nervous system. *Nature Reviews Neuroscience*, **4**, 121–130.
- Haas, H. L., Sergeeva, O. A., & Selbach, O. (2008). Histamine in the nervous system. *Physiological Reviews*, **88**, 1183–1241.
- Hammond, R. S., Lin, L., Sidorov, M. S., Wikenheiser, A. M., & Hoffman, D. A. (2008). Protein kinase a mediates activity-dependent Kv4.2 channel trafficking. *Journal of Neuroscience*, **28**, 7513–7519.
- Hoffman, D. A., & Johnston, D. (1998). Downregulation of transient K⁺ channels in dendrites of hippocampal CA1 pyramidal neurons by activation of PKA and PKC. *Journal of Neuroscience*, **18**, 3521–3528.
- Horn, R., & Marty, A. (1988). Muscarinic activation of ionic currents measured by a new whole-cell recording method. *Journal of General Physiology*, **92**, 145–159.
- Ito, C. (2000). The role of brain histamine in acute and chronic stresses. *Biomedicine & Pharmacotherapy*, **54**, 263–267.
- Johnston, D., Hoffman, D. A., Magee, J. C., Poolos, N. P., Watanabe, S., Colbert, C. M., & Migliore, M. (2000). Dendritic potassium channels in hippocampal pyramidal neurons. *Journal of Physiology*, **525**(Pt 1), 75–81.
- Kim, J., Jung, S. C., Clemens, A. M., Petralia, R. S., & Hoffman, D. A. (2007). Regulation of dendritic excitability by activity-dependent trafficking of the A-type K⁺ channel subunit Kv4.2 in hippocampal neurons. *Neuron*, **54**, 933–947.
- Kim, J., Wei, D. S., & Hoffman, D. A. (2005). Kv4 potassium channel subunits control action potential repolarization and frequency-dependent broadening in rat hippocampal CA1 pyramidal neurons. *Journal of Physiology*, **569**, 41–57.
- Kupchik, Y. M., Brown, R. M., Heinsbroek, J. A., Lobo, M. K., Schwartz, D. J., & Kalivas, P. W. (2015). Coding the direct/indirect pathways by D1 and D2 receptors is not valid for accumbens projections. *Nature Neuroscience*, **18**, 1230–1232.
- Lahiri, A. K., & Bevan, M. D. (2020). Dopaminergic transmission rapidly and persistently enhances excitability of D1 receptor-expressing striatal projection neurons. *Neuron*, **106**, 277–290.e6.
- Lin, L., Sun, W., Wikenheiser, A. M., Kung, F., & Hoffman, D. A. (2010). KChIP4a regulates Kv4.2 channel trafficking through PKA phosphorylation. *Molecular and Cellular Neuroscience*, **43**, 315–325.

- Ma, L., Jongbloets, B. C., Xiong, W. H., Melander, J. B., Qin, M., Lameyer, T. J., Harrison, M. F., Zemelman, B. V., Mao, T., & Zhong, H. (2018). A highly sensitive a-kinase activity reporter for imaging neuromodulatory events in awake mice. *Neuron*, **99**, 665–679.e5.
- Maffie, J. K., Dvoretzkova, E., Bougis, P. E., Martin-Eauclaire, M. F., & Rudy, B. (2013). Dipeptidyl-peptidase-like-proteins confer high sensitivity to the scorpion toxin AmmTX3 to Kv4-mediated A-type K⁺ channels. *Journal of Physiology*, **591**, 2419–2427.
- Mainardi, M., Spinelli, M., Scala, F., Mattera, A., Fusco, S., D'Ascenzo, M., & Grassi, C. (2017). Loss of leptin-induced modulation of hippocampal synaptic transmission and signal transduction in high-fat diet-fed mice. *Frontiers in Cellular Neuroscience*, **11**.
- Manz, K. M., Becker, J. C., Grueter, C. A., & Grueter, B. A. (2021). Histamine H3 receptor function biases excitatory gain in the nucleus accumbens. *Biological Psychiatry*, **89**, 588–599.
- McCormick, D. A., & Williamson, A. (1991). Modulation of neuronal firing mode in cat and guinea pig LGNd by histamine: Possible cellular mechanisms of histaminergic control of arousal. *Journal of Neuroscience*, **11**, 3188–3199.
- Mendonca, P. R. F., Kyle, V., Yeo, S. H., Colledge, W. H., & Robinson, H. P. C. (2018). Kv4.2 channel activity controls intrinsic firing dynamics of arcuate kisspeptin neurons. *Journal of Physiology*, **596**, 885–899.
- Miklos, I. H., & Kovacs, K. J. (2003). Functional heterogeneity of the responses of histaminergic neuron subpopulations to various stress challenges. *European Journal of Neuroscience*, **18**, 3069–3079.
- Munakata, M., & Akaïke, N. (1994). Regulation of K⁺ conductance by histamine H1 and H2 receptors in neurones dissociated from rat neostriatum. *Journal of Physiology*, **480**(Pt 2), 233–245.
- Nevarez, N., & de Lecea, L. (2018). Recent advances in understanding the roles of hypocretin/orexin in arousal, affect, and motivation. *F1000Res*, **7**, 1421.
- Norris, A. J., & Nerbonne, J. M. (2010). Molecular dissection of I(A) in cortical pyramidal neurons reveals three distinct components encoded by Kv4.2, Kv4.3, and Kv1.4 alpha-subunits. *Journal of Neuroscience*, **30**, 5092–5101.
- Panula, P., Chazot, P. L., Cowart, M., Gutzmer, R., Leurs, R., Liu, W. L., Stark, H., Thurmond, R. L., & Haas, H. L. (2015). International union of basic and clinical pharmacology. XCVIII. Histamine receptors. *Pharmacological Reviews*, **67**, 601–655.
- Panula, P., & Nuutinen, S. (2013). The histaminergic network in the brain: Basic organization and role in disease. *Nature Reviews Neuroscience*, **14**, 472–487.
- Pathak, D., Guan, D., & Foehring, R. C. (2016). Roles of specific Kv channel types in repolarization of the action potential in genetically identified subclasses of pyramidal neurons in mouse neocortex. *Journal of Neurophysiology*, **115**, 2317–2329.
- Pedarzani, P., & Storm, J. F. (1993). PKA mediates the effects of monoamine transmitters on the K⁺ current underlying the slow spike frequency adaptation in hippocampal neurons. *Neuron*, **11**, 1023–1035.
- Plenz, D., & Kitai, S. T. (1998). Up and down states in striatal medium spiny neurons simultaneously recorded with spontaneous activity in fast-spiking interneurons studied in cortex-striatum-substantia nigra organotypic cultures. *Journal of Neuroscience*, **18**, 266–283.
- Possieri, C., Locantore, P., Salis, C., Bacci, L., Aiello, A., Fadda, G., De Crea, C., Raffaelli, M., Bellantone, R., Grassi, C., Strigari, L., Farsetti, A., Pontecorvi, A., & Nanni, S. (2021). Combined molecular and mathematical analysis of long noncoding RNAs expression in fine needle aspiration biopsies as novel tool for early diagnosis of thyroid cancer. *Endocrine*, **72**, 711–720.
- Salgado, S., & Kaplitt, M. G. (2015). The nucleus accumbens: A comprehensive review. *Stereotactic and Functional Neurosurgery*, **93**, 75–93.
- Scala, F., Fusco, S., Ripoli, C., Piacentini, R., Li Puma, D. D., Spinelli, M., Laezza, F., Grassi, C., & D'Ascenzo, M. (2015). Intraneuronal Aβ accumulation induces hippocampal neuron hyperexcitability through A-type K(+) current inhibition mediated by activation of caspases and GSK-3. *Neurobiology of Aging*, **36**, 886–900.
- Schiffmann, S. N., Lledo, P. M., & Vincent, J. D. (1995). Dopamine D1 receptor modulates the voltage-gated sodium current in rat striatal neurones through a protein kinase A. *Journal of Physiology*, **483**(Pt 1), 95–107.
- Scotfield, M. D., Heinsbroek, J. A., Gipson, C. D., Kupchik, Y. M., Spencer, S., Smith, A. C., Roberts-Wolfe, D., & Kalivas, P. W. (2016). The nucleus accumbens: Mechanisms of addiction across drug classes reflect the importance of glutamate homeostasis. *Pharmacological Reviews*, **68**, 816–871.
- Selbach, O., Brown, R. E., & Haas, H. L. (1997). Long-term increase of hippocampal excitability by histamine and cyclic AMP. *Neuropharmacology*, **36**, 1539–1548.
- Shen, W., Hernandez-Lopez, S., Tkatch, T., Held, J. E., & Surmeier, D. J. (2004). Kv1.2-containing K⁺ channels regulate subthreshold excitability of striatal medium spiny neurons. *Journal of Neurophysiology*, **91**, 1337–1349.
- Shoblock, J., & O'Donnell, P. (2000). Histamine modulation of nucleus accumbens neurons. *Annals of the New York Academy of Sciences*, **909**, 270–272.
- Soria-Jasso, L. E., Bahena-Trujillo, R., & Arias-Montano, J. A. (1997). Histamine H1 receptors and inositol phosphate formation in rat thalamus. *Neuroscience Letters*, **225**, 117–120.
- Starodub, A. M., & Wood, J. D. (2000). Histamine H(2) receptor activated chloride conductance in myenteric neurons from guinea pig small intestine. *Journal of Neurophysiology*, **83**, 1809–1816.
- Steinberg, E. E., Boivin, J. R., Saunders, B. T., Witten, I. B., Deisseroth, K., & Janak, P. H. (2014). Positive reinforcement mediated by midbrain dopamine neurons requires D1 and D2 receptor activation in the nucleus accumbens. *Plos One*, **9**, e94771.
- Storm, J. F. (1987). Action potential repolarization and a fast after-hyperpolarization in rat hippocampal pyramidal cells. *Journal of Physiology*, **385**, 733–759.
- Surmeier, D. J., & Kitai, S. T. (1993). D1 and D2 dopamine receptor modulation of sodium and potassium currents in rat neostriatal neurons. *Progress in Brain Research*, **99**, 309–324.

- Takagi, H., Morishima, Y., Matsuyama, T., Hayashi, H., Watanabe, T., & Wada, H. (1986). Histaminergic axons in the neostriatum and cerebral cortex of the rat: A correlated light and electron microscopic immunocytochemical study using histidine decarboxylase as a marker. *Brain Research*, **364**, 114–123.
- Taylor, K. M., & Snyder, S. H. (1971). Brain histamine: rapid apparent turnover altered by restraint and cold stress. *Science*, **172**, 1037–1039.
- Tkatch, T., Baranauskas, G., & Surmeier, D. J. (2000). Kv4.2 mRNA abundance and A-type K(+) current amplitude are linearly related in basal ganglia and basal forebrain neurons. *Journal of Neuroscience*, **20**, 579–588.
- Xu, C., Michelsen, K. A., Wu, M., Morozova, E., Panula, P., & Alreja, M. (2004). Histamine innervation and activation of septohippocampal GABAergic neurones: Involvement of local ACh release. *Journal of Physiology*, **561**, 657–670.
- Yuan, W., Burkhalter, A., & Nerbonne, J. M. (2005). Functional role of the fast transient outward K+ current IA in pyramidal neurons in (rat) primary visual cortex. *Journal of Neuroscience*, **25**, 9185–9194.
- Zhang, L., & McBain, C. J. (1995). Potassium conductances underlying repolarization and after-hyperpolarization in rat CA1 hippocampal interneurons. *Journal of Physiology*, **488**(Pt 3), 661–672.
- Zhang, X. Y., Peng, S. Y., Shen, L. P., Zhuang, Q. X., Li, B., Xie, S. T., Li, Q. X., Shi, M. R., Ma, T. Y., Zhang, Q., Wang, J. J., & Zhu, J. N. (2020). Targeting presynaptic H3 heteroreceptor in nucleus accumbens to improve anxiety and obsessive-compulsive-like behaviours. *Proc Natl Acad Sci U S A*, **117**, 32155–32164.
- Zhou, F. W., Xu, J. J., Zhao, Y., LeDoux, M. S., & Zhou, F. M. (2006). Opposite functions of histamine H1 and H2 receptors and H3 receptor in substantia nigra pars reticulata. *Journal of Neurophysiology*, **96**, 1581–1591.
- Zhuang, Q. X., Xu, H. T., Lu, X. J., Li, B., Yung, W. H., Wang, J. J., & Zhu, J. N. (2018). Histamine excites striatal dopamine D1 and D2 receptor-expressing neurons via post-synaptic H1 and H2 receptors. *Molecular Neurobiology*, **55**, 8059–8070.

Additional information

Data availability statement

The datasets generated and/or analysed during the current study are available from the corresponding author on reasonable request.

Competing interests

All authors declare they have no competing interests/conflicts of interest related to this work.

Author contributions

G.A. and L.N. designed, performed and analysed electrophysiological experiments; C.C., A.B. and L.N. performed Western blot experiments; V.P., S.N. and G.A. performed high-quality single-cell RNA analysis by droplet digital PCR. M.D. and C.G. conceived the study, supervised the work and wrote the paper. All authors gave approval to the final version of the manuscript.

Funding

This work was supported by the Italian Ministry of University and Research (PRIN 2017-Prot. 2017K2NEF4 to M.D.) and Italian Ministry of Health, Ricerca Corrente – Fondazione Policlinico Universitario A. Gemelli IRCCS.

Acknowledgements

We thank Franziska M. Lohmeyer, PhD, Fondazione Policlinico Universitario A. Gemelli IRCCS, for her support in revising the manuscript. We also acknowledge the contribution of Electrophysiology Core Facility G-STeP, Fondazione Policlinico Universitario ‘A. Gemelli’ IRCCS.

Open Access Funding provided by Università Cattolica del Sacro Cuore within the CRUI-CARE Agreement.

Keywords

A-type potassium current, H2 receptor, histamine, intrinsic excitability, Kv4.2, nucleus accumbens

Supporting information

Additional supporting information can be found online in the Supporting Information section at the end of the HTML view of the article. Supporting information files available:

Statistical Summary Document

Peer Review History